

Reviewer 1:

Comments: This is the third paper from this group investigating the possibilities of deriving aerosol optical thickness at night from the VIIRS DNB. Interestingly I also reviewed the first paper in this series from 2013. I did not review or read the second paper in the series (McHardy et al., 2015) until I accepted this review. The group is making progress, but progress is slow. I would have hoped that they would have offered more than an incremental improvement to their 2015 paper, which is what we have here, and for awhile I was trying to determine whether this increment was sufficiently novel to warrant publication.

In this installment the authors implement a retrieval developed in the 2015 paper that uses the blurring of the spatial variability of light emitting city pixels at night to derive aerosol optical thickness (AOT). This is different from the paper that I reviewed in 2013 that used the contrast between the lit cities and the surrounding dark countryside. The idea of linking AOT to reduced sharpness of the image is old, and I am thinking of Tanré and Legrand (1991). The goal of a night time AOT from an imager is fundamentally ambitious. Everything from cloud clearing to the instability of artificial lights to the impossibility of collocating retrievals with current AERONET observations is working against you. Yet, the pay off is extremely rich, and as an aerosol product user, I am very happy that this group has not given up hope. The manuscript as it stands now could use some scrubbing to make it easier to understand, and I will make some recommendations. In some places the authors have made things complicated when simplicity should suffice. In particular the derivation of the cloud/aerosol free spatial variability measure for each target is complicated. It would also be helpful to start to quantify AOT accuracy using this method. Previous papers made that attempt, but here there was nothing. Overall the technique and implementation are sound, the presentation is sufficiently clean and the results sufficiently novel for publication. Therefore, I recommend publication after revision.

Tanré, D., & Legrand, M. (1991). On the satellite retrieval of Saharan dust optical thickness over land: Two different approaches. *Journal of Geophysical Research: Atmospheres*, 96(D3), 5221-5227.

Response: We thank the reviewer for his/her constructive comments and suggestions. Also, the focus of this paper is to study the variations of artificial light sources for various observational conditions as well as explore the potential of applying the method for regional retrievals. Note that the theoretical analysis of retrieval errors has been reported in McHardy et al. (2015), as mentioned by the reviewer. To quantify uncertainties, besides already attempted theoretical approaches, empirical approaches may be needed. This requires the comparison of VIIRS AOT with a benchmark AOD dataset. However, both daytime AERONET and nighttime CALIOP AOD data have their own issues, as mentioned in the paper and are not the best sources for estimating uncertainties empirically. Note that nighttime AOT data from AERONET have only recently become available, after the submission of this paper. Thus, we leave the validation efforts using nighttime AERONET data for a future paper. In this study, we included discussions on limitations of the study, hopefully adding a different angle for uncertainties of the study.

Point by point comments and recommendations.

Comments: Introduction. There are a few other groups besides this one that have attempted similar aerosol retrievals using the DNB, or investigated the possibility theoretically. In particular

I recommend referencing Wang et al. (2016), and possibly Choo and Jeong (2016), though the latter is very local in its scope. Wang et al. (2016) put to rest the importance of variable water vapor in the method. If they hadn't, I would be worried about that factor.

Wang, J., Aegerter, C., Xu, X., & Szykman, J. J. (2016). Potential application of VIIRS Day/Night Band for monitoring nighttime surface PM_{2.5} air quality from space.

Atmospheric Environment, 124, 55-63.

Choo, G. H., & Jeong, M. J. (2016). Estimation of nighttime aerosol optical thickness from Suomi-NPP DNB observations over small cities in Korea. Korean Journal of Remote Sensing, 32(2), 73-86.

Response: Thanks for the suggestions. We have cited the two papers.

Comments: Lines 88-95. I found the use of present tense “develops” (line 88) and “proposes” (line 90) a little odd. Those studies are done and published. I would have used “developed” and “proposed”, but I’m not sure this is required.

Response: Done.

Comments: What is the time span or dates of the study? Is it one year of data or multiple years? I don't see this stated anywhere.

Likewise no where is it stated that this is specifically Suomi-NPP VIIRS, because there are now more than one VIIRS flying. There's NOAA 20, and over the years there will be more.

Response: To avoid confusion, we have modified the following sentence to highlight the fact that only 2015 Suomi NPP VIIRS data were used.

“In this study, three processed and terrain-corrected Suomi NPP VIIRS datasets were used for 2015.”

Comments: The specific data sets look to me that they are IDPS data sets. IDPS processing and archiving of data sets has stopped or will stop very soon to be replaced by EPS data sets and processing. I think this should be clarified in the text.

Response: "VIIRS Cloud Cover Layers EDR (VCCLO) (public 04/27/2013)" and "VIIRS Day Night Band SDR (SVDNB) (public 02/07/2012)" were obtained between 9-2018 and 10-2018 from the Comprehensive Large Array-Data Stewardship System (CLASS) at <https://www.avl.class.noaa.gov/saa/products>.

We have added the following discussions in the paper.

The VIIRS data were obtained from the NOAA Comprehensive Large Array-Data Stewardship System (CLASS) site (<https://www.avl.class.noaa.gov/saa/products>)

Comments: Line 172 "attachment". First should this be "attachment" or "supplements"? Note that

I was unable to download or to see any of the supplementary files. This is likely a problem between me and the journal, not with the authors, but this should be tested.

Response: We changed from "attachment" to "supplements". Also, we checked MS Records for the paper and the above mentioned file was submitted to AMT on Dec. 14, 2018 as a supplement and is available for the corresponding author to download. We are unsure why the reviewer can't see the file. We will upload the file again..

Comments: Line 182. "optical depth". Elsewhere the authors use the term "optical thickness". It would be good to be consistent.

Response: Done.

Comments: Line 219. I believe the authors meant 0.6 to 1.0.

Response: Typo corrected. Thanks.

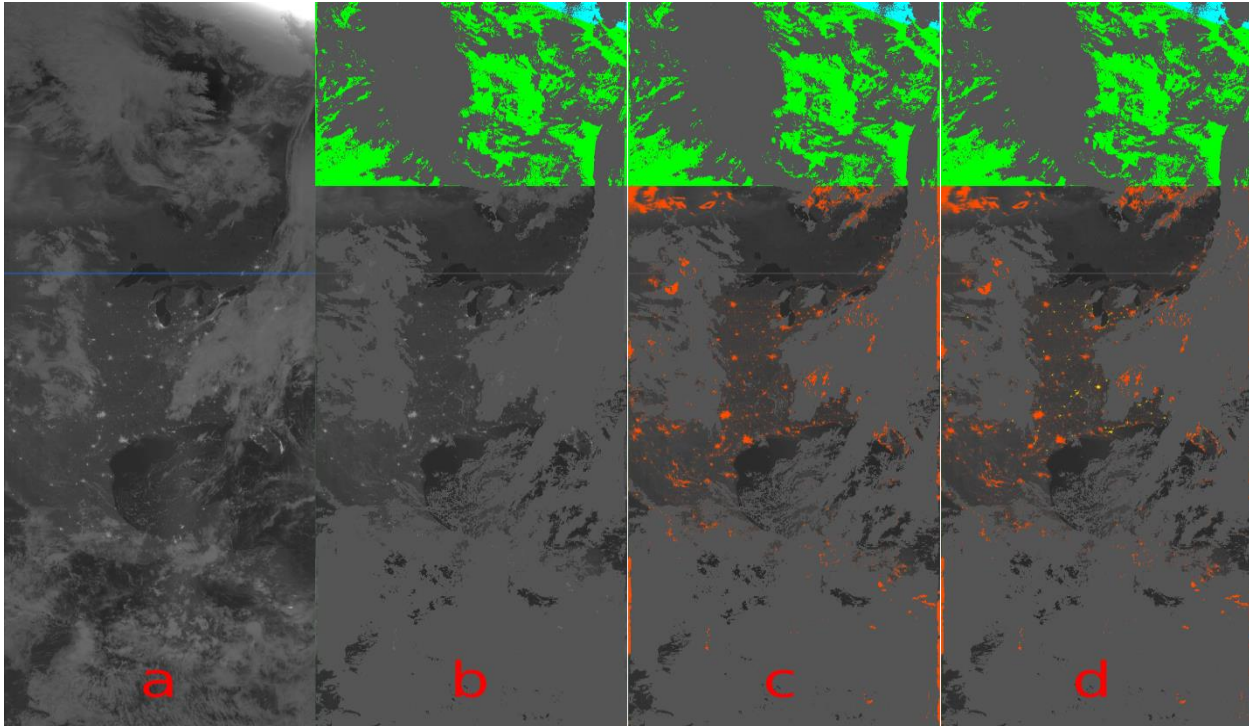
Comments: Beginning here the authors need greater clarity in their description of what was done. Lines 256-260. What does background mean? It seems that an a priori assessment has to be made. Or are the light emitting city pixels included in the mean cloud-free background pixels?

Response: Background means nearby non-artificial light source pixels. We have modified the sentence as:

"a given pixel to background pixels (non-artificial light pixels), as suggested in Johnson et al. (2013). "

Comments: Figure 2d. The green points are very hard to see. Would light blue be a better choice? Would it be better to use yellow for these pixels and green for signal saturation?

Response: Thank you for your suggestion. We made the changes. But since the cities are rather small we do not observe a significant improvement. Thus we kept the old figure.



Comments: Line 285 should be “retrievals”

Response: Done.

Comments: Line 286, “attached” again. “Supplement”?

Response: Done.

Comments: If the edges of the image correspond to the edges of the bounding box, please state so. If not, then draw the bounding box on the image.

Response: Thank you for your suggestion. We have added the revised figure, as suggested, to the paper.

Comments: Lines 295-304. In the discussion of cloud contamination and partly cloudiness there is no discussion of thin cirrus. There should be.

Response: We have revised the sentence to:

“Cloud contamination, especially cirrus cloud contamination, remains an issue in the above steps”

Comments: Line 309. Why the lopsided statistical cleaning? Dark Target aerosol algorithms do a symmetrical filtering over ocean in order to not impose a bias on the statistics. Over land the filtering is skewed because of bright surface pixels skew unfiltered biases towards too high AOD. Why the skewed filtering here?

Response: The lopsided statistical cleaning is applied as the histogram of radiance for a typical artificial light source is often non-Gaussian, and is biased towards lower radiance values. The non-Gaussian feature is the rationale behind a non-symmetrical filtering.

Comments: Lines 321 – 325. I’m not clear on this. Are you finding the mean for each green pixel? For each city of many pixels, so that first there is a spatial mean of all the green pixels and then a temporal mean to get the average over the time span? Or is this a spatial and then temporal mean for all the green pixels within the bounding box? Is there a difference between green pixels within a bounding box and the green pixels within a “city”. I have been assuming throughout the paper that standard deviation is a spatial standard deviation of all the green pixels either within a city or within a bounding box. This is supported at line 386. But here it could be a temporal stdev or an ensemble stdev from all cities on the particular Julian Day.

Response: For each artificial light source, there are countable artificial light source pixels (green pixels). Thus, for each night, for each artificial light source, the mean and the standard deviation of those artificial light source pixels for the given artificial light source are computed. Then, yearly means are computed from those daily estimations. Also, we assume green pixels within a bounding box represent green pixels within a “city”. We have added the following discussions to avoid confusion.

“Here, for each artificial light source (city/town), for a given satellite overpass of a given night, the mean radiance and the standard deviation of radiance for artificial light source pixels within the given city/town are computed, and are further used as the base elements for computing yearly mean radiance and standard deviation values.”

Comment: Line 329. Should that be $_{-0.1X N_STD}$? plus or minus?

Response: Here we used $N-0.1X N_STD$ to screening out nights with very low artificial light source pixels, mostly likely due to cloud coverage.

Comment: Line 346-349. This could be worded better. “non-totally cloudy” is clumsy. “nonovercast” is better. Though, “minimum number of non-overcast observations” is also clumsy. How about “June and July had the fewest acceptable observations”.

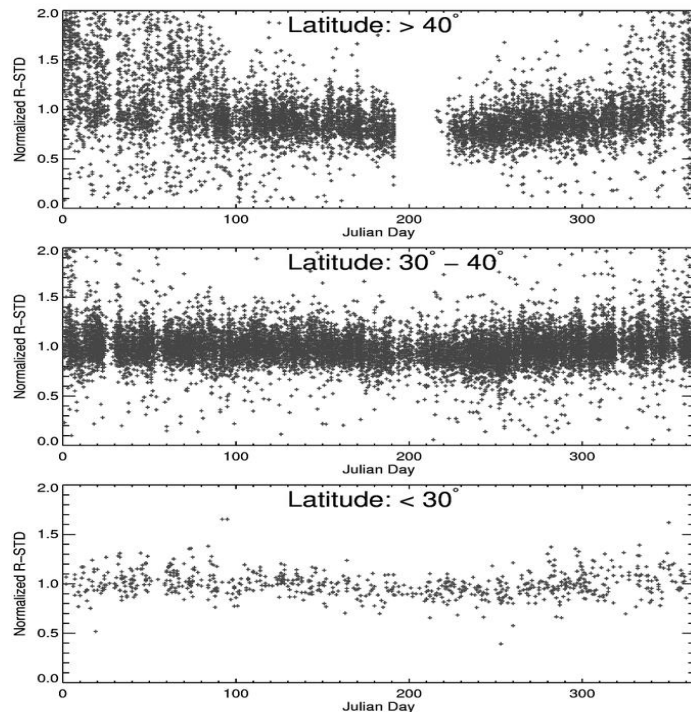
Response: We changed to “number of observations (cloud free or partially cloudy)”

Comment: Figures 4, 6,7,8,11 are not informative. How about density scatter plots? Or bin and average the data with standard deviation bars? Or calculate the regression statistics of those red lines in Figure 4? There will be additional comments on the scatter plot figures.

Response: We have added density scatter plots as suggested for Figures 4,6,7, and 8. For Figure 11, we reduced the symbol size. We have also added regression statistics in Figures 6,7, and 8.

Comment: Lines 365-367. There is a lot of discussion in the paper and speculation about snow contamination with no evidence to support the speculation. Could snowy and nonsnowy places (ie. California) be compared?

Response: Great question. We made the suggestion based on the figure below. Here we studied the normalized R-STD as a function of Julian day for three latitude ranges ($< 30^\circ$, $30-40^\circ$, and $> 40^\circ$). The high spikes are mostly found over high latitudes during wintertime. However, to fully study the impact of snow covered surfaces on this study, the topic may deserve a study of its own and thus we leave this for a future paper.



Comment: Lines 374 – 376. More on figures. That red line doesn't look like a good fit in Figures 4g and 4h, which makes the statements in these lines hard to accept. The red curves have a minimum around 30 deg, not nadir, so slant path length doesn't seem to be the best answer. This leaves anisotropic light sources. This is very interesting. Why?

Response: The red lines in Figures 4g and 4h are computed through second order regression / polynomial curve fitting. The above mentioned patterns are likely introduced by function fitting through a dataset with noisy data points.

Comment: Figure 5b. It would certainly be helpful to see some regression statistics.

Response: Done. We added the regression relationship to the figure.

Comment: Lines 399-408. The metric for DEL-Ia is complicated. The average stdev of the most variable 30% of the spatial stdevs, PLUS 2 stdevs of the stdevs of the most variable 30% of the spatial stdevs. I just don't see how this eliminates cloud contamination and lightning strikes. You have the top 1% of spatially variable light sources, but that top 1% will include clouds and lightning strikes. Also why can't you just use Rstd(1%) instead of finding mean and stdev of the top 30%.

Response: We tried to answer this question based on our understanding of the question. As the reviewer suggested, the top 1% may include cloud and lightning contamination, and thus Rstd(1%) could be biased. The use of the most variable 30% of the spatial stdevs is attempted in an effort to reduce this issue. As with more data samples included, uncertainties due to cloud and lightning contamination may be averaged out, resulting in a more statistically stable DEL-Ia estimation.

Comment: Lines 460-461. Regression slope is mentioned here. I know that there is a line of thought in the community that wants to get away from regression statistics, and so previously, even though I wanted to see regression statistics in the plots, I've refrained from demanding them. Except here regression slope is mentioned. If it is mentioned, then please show slopes, intercepts and R on the plots. If the regression is not linear, then show RMSE and R.

Response: We have added regression statistics in the plots as suggested.

Comment: Lines 471-472. These criteria will eliminate places with highly variable day-to-day changes in AOT.

*Response: We have added the following sentence to highlight the suggestion:
"Note that these criteria may exclude artificial light sources with highly variable day-to-day changes in AOT."*

Comment: Figure 7 is crying for a color density plot.

Response: Done.

Comment: Line 586. Sure for the U.S., but in other places the winter season might be fine.

*Response: We agreed. We have revised the sentence to:
“indicating the need for careful snow and ice detection for nighttime retrievals using VIIRS data
for regions that may experience snow/ice coverage. “*

Reviewer 2:

Comments: The paper "Characterization and application of artificial light sources for nighttime aerosol optical depth retrievals using the VIIRS Day/Night Band" deals with opportunities to detect and characterize aerosol at night by measuring visible radiance from city lights in VIIRS Day-Night band. The topic meets the aim and scopes of the journal.

The general structure of the paper is good.

The figures and its captions are of good quality.

The motivation and background are well reasoned in the introduction. It lists many relevant related papers. The presented research introduces novel concepts to use the relatively new DNB channel on VIIRS to use visible radiance during the night for aerosol characterization. This, if successful, could close the nighttime gap of aerosol observations by satellite-based retrievals.

Section 2.2 describes the theoretical approach. The aerosol optical depth retrieval is based on a comparison of spatial standard deviation under a cloud and aerosol-free conditions to the measured spatial standard deviation. For practical results, the authors describe filtering and data selection processes in a sufficient way.

The result section shows that this approach has some skill, but also still major limitations.

The authors discuss this in the concluding chapter and give suggestions for follow-up research.

I recommend minor revisions for the points specified in the next section.

Response: We thank the reviewer for his/her comments and suggestions.

Specific comments

Comments: Line 172: I can't find the full list of the cities in an attachment.

Response: We checked MS Records for the paper and the above mentioned file was submitted to AMT on Dec. 14, 2018 (supplement) and is available for the corresponding author to download. We are unsure why the reviewer can't see the file. We will upload the file again.

Comments: Line 305: "On each night and for each light source, the averaged radiance, its standard deviation.": What is here a light source? Can't be one individual DNB pixel. Is it a city (e.g. all green pixels in Fig.3b for Iowa City)?

Response: Yes, all green pixels in Fig. 3b represent valid artificial light source pixels for a given city. We have revised the sentence as:

"On each night and for each light source (e.g., a given city that is composed of multiple VIIRS DNB pixels such as shown in Fig. 3b), the averaged radiance, its standard deviation, the lunar fraction (fraction of the lunar disk illuminated by the sun, as viewed from Earth), viewing geometries, and the number of artificial light source pixels identified, are reported as diagnostic information."

Comments: Line 305: Define lunar fraction.

Response: We have revised the sentence as “the lunar fraction (fraction of the lunar disk illuminated by the sun, as viewed from Earth)”

Comments: Fig.11 and Equation 5: How can the transmission correction factor k as defined in Eq.5 be bigger than 1, as shown in Fig.11?

Response: It is introduced by uncertainties in various factors, such as uncertainties in ΔI_a and CALIOP AOT.

1
2
3
4
5
6
7
8
9
10
11
12
13
14
15
16
17
18
19
20
21
22
23
24
25
26
27
28
29
30
31
32
33
34
35
36
37
38
39
40
41
42
43
44
45
46
47
48

Characterization and application of artificial light sources for nighttime aerosol optical depth retrievals using the VIIRS Day/Night Band

Jianglong Zhang¹, Shawn L. Jaker¹, Jeffrey S. Reid², Steven D. Miller³, Jeremy Solbrig³, and Travis D. Toth⁴

¹Department of Atmospheric Sciences, University of North Dakota, Grand Forks, ND, USA

²Marine Meteorology Division, Naval Research Laboratory, Monterey, CA, USA

³Cooperative Institute for Research in the Atmosphere, Colorado State University, Fort Collins, CO, USA

⁴NASA Langley Research Center, Hampton, VA, USA

Submitted to
Atmospheric Measurement Techniques

03 Dec. 2018

Corresponding Author: jzhang@atmos.und.edu

49 **Abstract**

50
51 Using nighttime observations from Visible/Infrared Imager/Radiometer Suite (VIIRS) Day/Night
52 band (DNB), the characteristics of artificial light sources are evaluated as functions of observation
53 conditions and incremental improvements are documented on nighttime aerosol retrievals using
54 VIIRS DNB data on a regional scale. We find that the standard deviation of instantaneous radiance
55 for a given artificial light source is strongly dependent upon the satellite viewing angle, but is
56 weakly dependent on lunar fraction and lunar angle. Retrieval of nighttime aerosol optical
57 thickness (AOT) based on the novel use of these artificial light sources is demonstrated for three
58 selected regions (United States, Middle East, and India) during 2015. Reasonable agreements are
59 found between nighttime AOTs from VIIRS DNB and temporally adjacent daytime AOTs from
60 Aerosol RObotic NETwork (AERONET) as well as from coincident nighttime AOT retrievals
61 from the Cloud-Aerosol Lidar with Orthogonal Polarization (CALIOP), indicating the potential of
62 this method to begin filling critical gaps in diurnal AOT information at both regional and global
63 scales. Issues related to cloud, snow, and ice contamination during the winter season, as well as
64 data loss due to the misclassification of thick aerosol plumes as clouds, must be addressed to make
65 the algorithm operationally robust.

66 **1 Introduction**

67 The Visible/Infrared Imager/Radiometer Suite (VIIRS), on board the Suomi National Polar-
68 orbiting Partnership (NPP) satellite, features 22 narrow-band channels in the visible and infrared
69 spectrum. Included on VIIRS is the Day/Night band (DNB), designed to detect both reflected
70 solar energy at daytime and low light visible/near-infrared signals at nighttime (e.g., Lee et al.,
71 2006; Miller et al., 2013; Elvidge et al., 2017). Compared to the Operational Line Scan (OLS)
72 sensor on the legacy Defense Meteorological Satellite Program (DMSP) constellation, the VIIRS
73 DNB has improved response to nighttime visible signals, owing to its higher spatial resolution,
74 radiometric resolution, and sensitivity (e.g., Miller et al., 2013; Elvidge et al., 2017). The DNB,
75 unlike the OLS, is calibrated which enables quantitative characterization of nighttime
76 environmental parameters via a variety of natural and artificial light signals, including reflected
77 moon light in cloudy and cloud free regions, natural and anthropogenic emissions from forest fires,
78 volcanic eruptions, gas flares from oil fields, and artificial light sources from cities (e.g., Miller et
79 al., 2013; Elvidge et al., 2017).

80 Using nighttime observations from VIIRS/OLS over artificial light sources such as cities,
81 several studies have attempted to derive nighttime aerosol optical properties. For example, Zhang
82 et al. (2008) propose the concept of estimating nighttime aerosol optical thickness (AOT) by
83 examining changes in DMSP/OLS radiances over artificial light sources between aerosol free and
84 high aerosol loading (and cloud-free) nights. However, the OLS visible channel does not have on-
85 board calibration, which limits the use of OLS data for quantitative studying of nighttime aerosol
86 properties. VIIRS's improved spatial and spectral resolutions and on-board calibration make
87 accurate quantification of nighttime aerosol properties feasible.

88 Using VIIRS radiances over selected artificial light sources, Johnson et al. (2013) developed a
89 retrieval of nighttime AOT for selected cities. However, radiances from artificial light-free regions
90 are needed for this retrieval process. McHardy et al. (2015) proposed an improved method, based
91 on the method proposed by Johnson et al. (2013) which uses changes in spatial variations within
92 a given artificial light source for retrieving nighttime AOT. The advantage of McHardy et al.
93 (2015) is that only observations over the artificial light sources themselves are needed, eliminating
94 the need for artificial light-free regions and implicit spatial invariance assumptions of Johnson et
95 al. (2013). Following those early attempts, several other studies have also explored the potentials
96 of applying similar methods for air quality studies, and for applying it to small cities [e.g., Choo
97 and Jeong, 2016; Wang et al., 2016].

Deleted: s

Deleted: Inspired by these pioneering efforts

Deleted: y

Deleted: ; Choo and Jeong, 2016

98 As proof-of-concept studies, only a few selected artificial light sources have been considered
99 in those pioneering nighttime aerosol retrieval studies that utilize VIIRS observations. As
100 suggested from McHardy et al. (2015), careful studies of the characteristics of artificial light
101 sources are needed to apply the method over a broader domain. Thus, in this study, using VIIRS
102 data from 2015 over the US, Middle East, and India, we focus on answering the following
103 questions:

- 104 (1) How do radiance fields from artificial light sources vary as functions of observing
105 conditions?
- 106 (2) Are nighttime AOT retrievals using VIIRS DNB feasible on a regional basis? In
107 particular, for our selected regions, can reasonable agreement be achieved between
108 nighttime VIIRS DNB derived AOT, aerosol retrievals from Cloud-Aerosol Lidar with
109 Orthogonal Polarization (CALIOP), and approximated nighttime AOT values from
110 daytime AErosol RObotic NETwork (AERONET)?

115 (3) What are the limitations in the current approach that can be improved in future attempts?

116 In the current study, we do not aim to finalize the nighttime retrieval methods, but rather
117 explore existing issues, report incremental advancements, and propose revised methods for future
118 studies. This paper is organized as follows: Section 2 introduces the datasets used in this study as
119 well as data processing and aerosol retrieval methods. Section 3 discusses artificial light source
120 patterns as functions of viewing and lunar geometries and lunar fraction, as well as other
121 observation-related parameters. Results of regional-based retrievals are also included in Section
122 3. Section 4 closes the paper with discussion and conclusions.

123

124 **2 Datasets and Methods**

125 **2.1 Datasets**

126 Flying in a sun-synchronous polar orbit, VIIRS has a local nighttime overpass time of ~1:30
127 am. The spatial resolution of a VIIRS DNB pixel is ~750 m across the full swath width of ~3000
128 km. VIIRS DNB observes at a wavelength range of 0.5 - 0.9 μm , with a peak wavelength of ~0.7
129 μm (e.g., Miller et al., 2013). VIIRS differs from its ancestor, OLS, by providing on-board
130 calibration for tracking signal degradation as well as changes in modulated spectral response
131 function through the use of a solar diffuser (e.g., Chen et al., 2017). Early versions of VIIRS DNB
132 data suffer from stray light contamination (e.g., Johnson et al., 2013). These issues have since
133 been corrected for in the later version of the VIIRS DNB data (Mills et al., 2013).

134 In this study, three processed and terrain-corrected [Suomi NPP](#) VIIRS datasets were used [for](#)
135 [2015](#). The VIIRS/DNB Sensor Data Record (SVDNB) includes calibrated VIIRS DNB radiance
136 data for the study as well as Quality Assurance (QA) flags for each pixel. The VIIRS Cloud
137 Cover/Layers Environmental Data Record (VCCLO) dataset was used for cloud clearing, and the

138 VIIRS/DNB Sensor Data Record Ellipsoid Geolocation (GDNBO) dataset was used for obtaining
139 geolocation for the VIIRS DNB radiance data. The GDNBO dataset also includes other ancillary
140 parameters including solar, lunar, and satellite zenith/azimuth angles, as well as lunar phase that
141 were used as diagnostic information in support of this study. [The VIIRS data were obtained from](https://www.avl.class.noaa.gov/saa/products)
142 [the NOAA Comprehensive Large Array-Data Stewardship System \(CLASS\) site](https://www.avl.class.noaa.gov/saa/products)
143 [\(https://www.avl.class.noaa.gov/saa/products\).](https://www.avl.class.noaa.gov/saa/products)

144 To evaluate the VIIRS retrieved AOTs, cloud-cleared and quality-assured Level 2, Version 3
145 AEROSOL ROBOTIC NETWORK (AERONET) data were enlisted as the “ground truth.” Reported in
146 AERONET data are AOTs at a typical wavelength range of 0.34 to 1.64 μm (Holben et al., 1998).
147 We point out that AERONET AOTs are derived through measuring the attenuation of solar energy
148 at defined wavelengths, and thus are only available during daytime. Therefore, averaged AOTs
149 (0.675 μm) for the day before and after the VIIRS observations were used in evaluating the
150 performance of VIIRS retrievals at night. A pair of VIIRS and AERONET retrievals are
151 considered collocated if the temporal difference is within ± 24 hours and the spatial difference is
152 within 0.4° Latitude/Longitude. All collocated AERONET data for one VIIRS data point were
153 averaged to represent the AERONET-retrieved AOT value of the desired VIIRS retrieval.

154 Nighttime aerosol retrievals are also available from CALIOP aerosol products at both regional
155 and global scales and for both day and nighttime (Winker et al., 2007). Thus, we also inter-
156 compared VIIRS nighttime AOTs retrieved from this study with CALIOP column integrated
157 AOTs. The Version 4.10, Level 2 CALIOP aerosol profile products (L2_05kmAPro) were used
158 in this study. Upon quality assurance steps, as mentioned in Toth et al. (2018), column integrated
159 CALIOP AOTs were derived at the 0.532 and 1.064 μm channels and then interpolated to the 0.70
160 μm channel (central wavelength of the DNB) for this study. The VIIRS and CALIOP data pair is

161 considered to be collocated if the spatial difference was within 0.4° Latitude/Longitude and the
162 temporal difference was within ± 1 hour. Note that one VIIRS retrieval may be associated with
163 multiple CALIOP AOT retrievals, and thus collocated CALIOP aerosol retrievals were averaged
164 to a single value for this comparison.

165 An open-source global city database from MaxMind (<http://www.maxmind.com/>) was used in
166 this study for cross checking with the detected artificial light sources for this study. The city
167 database includes the name and geolocation of the cities as well as other ancillary information.
168 Based on these data, a total of 999 cities from the Middle East region (11-42°N, 28-60°E) and
169 2995 cities from the India region (8-35°N, 68-97°E) were used in this study. These cities, as well
170 as their geolocations, are shown in Figs. 1b and 1c for the Middle East and India regions,
171 respectively, and are documented and attached as appendices to this paper.

172 One focus of this study is to understand the variations of artificial light sources as a function
173 of observing conditions. To achieve this goal, we have arbitrarily selected 200 cities across the
174 US. Since aerosol loadings are relatively low in the US compared to regions such as the Middle
175 East and India, this selection gives insight into the characteristics of artificial light sources. Also,
176 we require the selected cities to be isolated – that is, not in the immediate vicinity of another city
177 or major light source, so as to avoid light dome contamination. The majority of selected cities
178 have populations within the range of 25,000 and 100,000 with a few higher-population exceptions
179 such as Memphis, New Orleans, and Charleston. The geolocations of the 200 cities are shown in

180 Fig. 1a, and as mentioned above, the full list of the cities are also included as supplements,

181

182 2.2 Retrieval methods

Deleted: an

Deleted: attachment

185 The theoretical basis for retrieving nighttime AOT using stable artificial lights is based upon
 186 previous studies (Zhang et al., 2008; Johnson et al., 2013; McHardy et al., 2015). In the current
 187 approach, the VIIRS-observed radiance over a cloud free artificial light source can be expressed
 188 as:

$$I_{sat} = I_s e^{-\tau/\mu} + I_s T(\mu) + I_p \quad (1)$$

189 Where I_{sat} is the satellite received radiance, represented as the sum of contributions from three
 190 principal components: upwelling surface light emission through direct ($I_s e^{-\tau/\mu}$) and diffuse ($I_s T(\mu)$)
 191 transmittance, and the path radiance source term (I_p). Here, τ is the total column optical thickness,
 192 from aerosol and Rayleigh components, μ is the cosine of the viewing zenith angle, and $T(\mu)$ is
 193 the diffuse-sky transmittance. I_s is the cloud free sky surface upward radiance, which can be
 194 further rewritten as:
 195

$$\pi \bar{I}_s = r_s (\mu_0 F_0 e^{-\tau/\mu_0} + \mu_0 F_0 T(\mu_0) + \pi \bar{r}) + \pi \bar{I}_a \quad (2)$$

196 Where r_s , μ_0 , F_0 are (respectively) the surface reflectance, cosine of the lunar zenith angle, and
 197 the top-of-atmosphere downward lunar irradiance convolved with the VIIRS DNB response
 198 function. $T(\mu_0)$ is the diffuse transmittance term, \bar{r} is the reflectance from the aerosol layer, and
 199 I_a is the emission from the artificial light source. The three terms inside the parentheses of Eq. 2
 200 comprise the surface downward irradiance terms, where $\mu_0 F_0 e^{-\tau/\mu_0}$ is the downward irradiance from
 201 moonlight through direct attenuation (or $F_{directdown}$) and $\mu_0 F_0 T(\mu_0)$ is the downward irradiance from
 202 moonlight through diffuse transmittance (or $F_{diffusedown}$). The $\pi \bar{r}$ term represents the surface
 203 emission (irradiance) that is reflected back downward to the surface by the aerosol layer that has
 204 a layer mean reflectivity of \bar{r} . Eq. 2 shows that the surface emission term includes emission from
 205

Deleted: aerosol optical thickness

Deleted: depth

Deleted: depth

209 the artificial light source, as well as from reflected downward fluxes. Solving I_s from Eq. 2,
 210 inserting that result into Eq. 1, and rearranging, yields:

$$I_{sat} = \frac{r_s(F_{directdown} + F_{diffusedown}) + \pi I_a}{\pi(1 - r_s \bar{r})} [e^{-\tau/\mu} + T(\mu)] + I_p \quad (3)$$

211
 212
 213
 214 We expect the artificial light source emission term, I_a , to vary spatially within a heterogeneous
 215 light source such as a larger city. Within that city, we can assume that the $F_{directdown}$, $F_{diffusedown}$,
 216 and I_p terms have negligible spatial variations. This assumption follows McHardy et al. (2015),
 217 who also assume the surface diffuse emission term ($I_s T(\mu)$) is spatially invariant. However, as
 218 indicated in Eq. 3, the surface diffuse emission term includes the I_s , which contains the I_a term.
 219 Thus, we retain the surface diffuse emission term in this study.

220 By taking the spatial derivative of Eq. 3 (using the delta operator Δ) and by eliminating terms
 221 that have small variation within a city, we can derive:

$$\Delta I_{sat} = \frac{\Delta I_a}{1 - r_s \bar{r}} [e^{-\tau/\mu} + T(\mu)] \quad (4)$$

223 The ΔI_a and ΔI_{sat} are the spatial variance in TOA radiance within an artificial light source for
 224 aerosol and cloud free, and cloud free conditions, respectively. Similar to McHardy et al. (2015),
 225 the spatial variance in radiance in this study is represented by the standard deviation of radiance
 226 within an artificial light source. Also, the diffuse transmittance, $T(\mu)$, is required. Following
 227 Johnson et al. (2013), we estimated the ratio (k) between direct transmittance ($e^{-\tau/\mu}$) and total
 228 transmittance using the 6S radiative transfer model (Vermote et al., 1997). This approach can also
 229 be shown as Eq. 5:

$$k = e^{-\tau/\mu} / [e^{-\tau/\mu} + T(\mu)] \quad (5)$$

231 The look-up-table (LUT) values of k were computed for the AOT ranges of 0-1.5 (with every 0.05 AOT
 232 interval for AOT < 0.6 and for every 0.1 AOT interval for AOT of 0.6-1.0, and with two high AOT values

Deleted: 0.

234 of 1.2 and 1.5), for three different aerosol types: dust, smoke, and pollutants. We also modified the 6S
235 model (Vermote et al., 1997) to account for the spectral response function of the VIIRS DNB band (e.g.,
236 Chen et al., 2017). No sea salt aerosol was included in the LUT for this study, as artificial light sources
237 considered in this study were inland with less probability of sea salt aerosol contamination. Still, sea salt
238 aerosol can be added in later studies. Thus, we can rewrite Eq. 4 as:

$$239 \quad \tau = \mu \ln \frac{\Delta I_a}{k \Delta I_{sat}(1 - \bar{r}r_s)} \quad (6)$$

240
241 As suggested from Eq. 6, nighttime column optical thickness (τ) can be estimated using spatial
242 variances of an artificial light source over aerosol- and cloud-free conditions. The $\bar{r}r_s$ term arises from
243 the reflectance between the aerosol and the surface layers. This term is small for dark surfaces or
244 low aerosol loading cases, but could be significant for thick aerosol plumes over bright surfaces,
245 such as dust aerosols over the desert. We assume this term is negligible for this study. Note that
246 τ values from Eq. 6 include AOT as well as scattering (Rayleigh) and absorption (e.g., oxygen A
247 band) optical depth from gas species. To derive nighttime AOTs, 6S radiative transfer calculations
248 (Vermote et al., 1997) were used, assuming a standard atmosphere, to compute and remove the
249 component due to molecular scattering.

250 251 **2.3 Data pre-processing steps**

252
253 The VIIRS data pre-processing for nighttime aerosol retrievals is implemented through two
254 steps. First, artificial light sources are identified. Second, the detected artificial light sources are
255 evaluated against a known city database and a detailed regional analysis is performed. This latter
256 step is necessary to eliminate any unwanted “false” artificial light sources such as cloud
257 contamination or lightning strikes.

258 In the first step, conducted on individual ‘granules’ (~90 second orbital subsets) or composites
259 of adjacent granules, artificial light sources are selected after cloud screening and quality assurance

260 procedures. Since VIIRS nighttime aerosol retrievals assume cloud free conditions, cloud-
261 contaminated pixels must be removed using the VIIRS cloud products. Note that the nighttime
262 VIIRS cloud mask is thermal infrared based, and has its limitations in detecting low clouds
263 (especially over land), and thus additional cloud screening methods are also implemented as
264 mentioned in a later section. A single granule of VIIRS DNB radiance data is 4064 by 768 pixels
265 while, for the same VIIRS granule, the VIIRS cloud product reports values at 2032 by 384 pixels.
266 Thus, the VIIRS cloud product is first oversampled and then used to screen the radiance data.
267 Following the cloud screening step, VIIRS DNB Quality Assurance (QA) flags are used to
268 eliminate pixels that either have missing or out-of-range data, exhibit saturation, or have bad
269 calibration quality. We require the solar zenith angle to be larger than 102° to eliminate solar
270 (including twilight) contamination. Upon cloud screening and QA checks, artificial light pixels
271 are detected using a threshold based method by examining the difference in radiance of a given
272 pixel to background pixels (non-artificial light pixels), as suggested in Johnson et al. (2013).
273 Artificial light pixels are defined as pixels having radiance values greater than 1.5 times that of the
274 granule or multi-granule mean cloud-free background radiances.

275 The implementation of the first pre-processing step is illustrated in Figs. 2a-2d. Figure 2a
276 shows VIIRS DNB radiance data over North America for Oct. 1, 2015. Figure 2b shows the same
277 data as Fig. 2a but with cloud screening (shown in gray) and QA steps applied. Data removed by
278 the day/night terminator (i.e., solar zenith angle $< 102^\circ$) are shown in cyan, and pixels with QA
279 values indicating signal saturation are shown in yellow. Pixels in orange color in Fig. 2c are the
280 detected potential light sources on the granule scale. As shown in Fig. 2c, some cloud pixels may
281 still be misclassified as artificial light sources. To avoid such false detection, the detected artificial
282 light sources are further evaluated against a list of known cities for a given region as mentioned in

Deleted: le

284 Section 2. This step is shown in Fig. 2d, where green colored pixels are artificial light sources
285 confirmed by the known city light source database. Here, only 200 arbitrarily selected cities in the
286 US were used, and thus some of the artificial light sources, although positively identified, were
287 not highlighted in green as they were not in the city list.

288 The granule or multi-granule mean cloud-free background radiances are used for detecting
289 artificial light sources in the first step, which may introduce an over- or under-detection of artificial
290 light sources. To refine this detection, a regionally based artificial light source detection step is
291 implemented. In this step, a bounding box is selected for each cloud-free city. The bounding
292 boxes are manually selected for 200 cities in the US and 8 cities in the Middle-East. Based on
293 experimenting, we found that most cities have a bounding box size of less than $\pm 0.3^\circ$
294 latitude/longitude, except for large cities that have a population of ~quarter-million or more,
295 depending on countries. Thus, for the remaining 991 cities in the Middle-East and 2995 cities in
296 India, to simplify the process, a $\pm 0.3^\circ$ latitude/longitude region was picked as the bounding box.
297 The bounding boxes for large cities need to be manually selected in future studies.

298 Even if a city is partially included in a bounding box, or multiple cities reside within a bounding
299 box, retrievals can still be performed, since variances of detected artificial light sources are used
300 for aerosol retrievals regardless of origins of those artificial light sources. The latitude and
301 longitude ranges of the bounding boxes for all cities used in the study are included in the
302 [Supplement](#). Similar steps as mentioned in the granule or multi-granule level detection scheme
303 are implemented here, but with the use of localized mean cloud-free background radiances. The
304 results from the regional detection is shown in Fig. 3. Figure 3a is the VIIRS nighttime image for
305 Sioux City, Iowa for April 13, 2015. The detected artificial light sources are shown in Fig. 3b,
306 where pixels with green color represent artificial light sources that are identified based on the local

Deleted:

Deleted: s

Deleted: of attached city list files

310 detection scheme (the second step) while the pixels with orange color represent pixels identified
311 at the granule or multi-granule level (the first step) but fail on regional detection or outside the
312 bounding box.

313 Cloud contamination, especially cirrus cloud contamination, remains an issue in the above
314 steps, as shown in Fig. 2c, owing to limitations in the VIIRS infrared-based nighttime cloud mask.

Deleted: Cloud contamination, and especially cirrus cloud contamination, remains an issue in the above steps

Formatted: Font: Not Bold, Not Italic

315 To further eliminate cities that are partially covered by clouds, for a given artificial light source,
316 nights with mean latitudes and longitudes from detected light source pixels that are larger than
317 0.02° of the seasonally or yearly mean geolocations are excluded. This process is based on the
318 assumption that for a partially cloud covered city, only a portion of the city is detected as artificial
319 light source, and thus the mean geolocations likely deviate from the multi-night composited mean
320 geolocations. However, this step may misidentify heavy aerosol plumes as cloud contaminated
321 scenes. These nuances of city light identification remain a topic of ongoing research, and for now
322 remain as an outstanding source of uncertainty in the current retrieval algorithm.

323 On each night and for each light source (e.g., a given city that is composed of multiple VIIRS
324 DNB pixels such as shown in Fig. 3b), the averaged radiance, its standard deviation, the lunar
325 fraction (fraction of the lunar disk illuminated by the sun, as viewed from Earth), viewing
326 geometries, and the number of artificial light source pixels identified, are reported as diagnostic
327 information. To further avoid contamination from potential cloud / surface contaminated pixels,

Formatted: Font: Not Bold, Not Italic

328 or from pixels with erroneously high radiance values due to lightning flashes, in the process of
329 computing standard deviation the top 0.5% and bottom 10% of pixels are excluded. Finally, this
330 dataset is further used in the retrieval process.

Deleted: On each night and for each light source (e.g., a given city that is composed of multiple VIIRS DNB pixels such as Fig. 3b), the averaged radiance, its standard deviation, the lunar fraction (fraction of sun illuminated moon), viewing geometries, and the number of artificial light source pixels identified, are reported as diagnostic information.

331

340 **3. Results**

341 **3.1. Linkages between artificial lights and observing conditions**

342 As mentioned in Section 2, 200 cities within the US were arbitrarily chosen to examine the
343 properties of artificial light sources, as we expect less significant aerosol contaminations over the
344 US in comparison to other regions considered in this study. This analysis allows us to gain insight
345 on the natural variations of artificial light sources as a function of various observing parameters—
346 variations that will determine the inherent uncertainty of aerosol retrievals.

347 Cities have varying spatial light patterns, populations, and nighttime electricity usage, as well
348 as different surface conditions. To study the overall impacts of the observing conditions on
349 artificial light source patterns, the yearly mean radiance and standard deviation of the detected

350 light sources were computed for each city, regardless of observing conditions. Here, for each
351 artificial light source (city/town), for a given satellite overpass of a given night, the mean radiance
352 and the standard deviation of radiance for artificial light source pixels within the given city/town
353 are computed, and are further used as the base elements for computing yearly mean radiance and
354 standard deviation values. Then, for each city and for each night, the instantaneous radiance and

355 standard deviation values were scaled based on yearly mean values to derive a yearly mean
356 normalized radiance (N_Radiance) and standard deviation (N_R_{std}). This process was necessary
357 to remove city-specific characteristics, making feasible the comparison of artificial light source
358 properties from different cities. Also, to remove nights with cloud contamination or bad data, the
359 yearly mean (N) and standard deviation (N_STD) of the total number of light source pixels
360 identified for a given artificial light source was computed. Only nights with a number of detected
361 light source pixels exceeding $N - 0.1 \times N_STD$ were used in the subsequent analysis.

Deleted: Here, for each artificial light source (city/town), for a given satellite overpass of a given night, the mean radiance and the standard deviation of radiance for artificial light source pixels within the given city/town are computed, and are further used to as the base elements for computing yearly mean radiance and standard deviation values.

Formatted: Font: Not Italic

Deleted:

369 Figure 4a shows the plot of Julian day versus normalized radiance using data from all 200
370 cities on all available nights, regardless of the observing conditions (with the exception of totally
371 cloudy scenes, as identified by the VIIRS cloud product, which were removed). As suggested
372 from Fig. 4a, nighttime artificial light sources vary as a function of Julian day. Higher radiance
373 values were found over the Northern Hemisphere winter season (Julian days greater than 300 or
374 less than 100, corresponding to the months of November through March of the following year),
375 compared to the Northern Hemisphere spring, summer, and fall seasons. In particular, during the
376 Northern Hemisphere winter season, high spikes of radiance values were clearly visible. The
377 increase in radiance values as well frequent high spikes in radiance values during the winter season
378 may be due in part to snow and ice reflectance (modifying the surface albedo, and hence the
379 multiple scatter between the atmosphere and surface as well as augmented lunar reflectance),
380 especially for high latitude regions. Thus, snow and ice removal steps are needed for nighttime
381 aerosol retrievals on both regional and global scales. Still, upon characterizing the snow/ice cover
382 from daytime observations, retrievals may still be possible over snow/ice contaminated regions for
383 future studies.

384 Also apparent in Fig. 4a is variation in the number of observations (cloud free or partially
385 cloudy) with respect to Julian day. The minimum number of cloud-free or partially cloudy
386 observations that passed the QA checks occurs during the months of June and July, likely due to
387 saturation QA-flagged pixels (colored in yellow in Fig. 2) reaching the furthest south during those
388 two months. VIIRS DNB QA checks also label a block of pixels adjacent to the day/night
389 terminator as pixels with bad QA (e.g., the yellow colored area in Fig. 2b). Thus, during June and
390 July, a significant portion of artificial light sources at high latitudes were removed from the
391 analysis. These QA steps are retained in the process, although relaxing these QA requirements

Deleted: non-totally cloudy

Deleted: non-overcast

394 may be an option for enhancing data volume over high latitudes. An assessment of the
395 uncertainties incurred by reducing the conservative nature of the QA flag is a subject of future
396 studies.

397 Figures 4c and 4e show that the yearly mean normalized radiance, $N_Radiance$, varies as a
398 function of lunar status, including the lunar fraction and lunar zenith angle. As the lunar fraction
399 increases, the $N_Radiance$ increases, possibly due to the increase in reflected moon light. As lunar
400 zenith angle increases (i.e., the moon is less high in the sky), a decrease in the $N_Radiance$ is
401 found, indicating a reduction in downward moon light as lunar zenith angle increases. An
402 interesting relationship between the $N_Radiance$ and satellite zenith angle emerges in Fig. 4g. A
403 10-20% increase in $N_Radiance$ is observed for an increase of satellite zenith angle from 0 to 60°.

404 Figures 4b,d,f,h show similar analyses as Figs. 4a,c,e,g but for N_R_{std} . A similar relationship
405 between N_R_{std} and Julian day is also found, with larger N_R_{std} values found in winter and smaller
406 values found in the summer. Also, larger spikes of N_R_{std} , possibly due to snow and ice
407 contamination, are found in the winter season, suggesting that careful ice and snow detection
408 methods are needed for processing VIIRS DNB data over high latitudes during the winter season.
409 Still, the increase in nighttime radiance and standard deviation of radiance may also be due to the
410 increase in artificial light usage at night during the winter months, and for this reason, seasonal or
411 monthly based ΔI_a values may be needed. In contrast to the normalized radiance, insignificant
412 changes in N_R_{std} were observed with the varying of either lunar fraction or lunar zenith angle,
413 indicating that lunar fraction or lunar zenith angle have less impact on nighttime aerosol retrievals
414 when considering N_R_{std} .

415 N_R_{std} was found to be strongly dependent upon the satellite zenith angle, with values larger
416 than 1 observed at near 60° viewing zenith angle, likely due to the anisotropic behavior of artificial

417 light sources, as well as longer slant paths although the true reason remains unknown. To account
418 for this viewing zenith angle dependency, a correction factor c was introduced in Johnson et al.
419 (2013) in anticipation of this result. Based on Fig. 4h, the correction factor, c , specified as a
420 function of the satellite viewing zenith angle (θ), was calculated using VIIRS DNB data from 2015
421 over the 200 selected cities:

$$422 \quad c = 1.66 - 1.75 \times \cos(\theta) + 0.91 \times \cos(\theta)^2 \quad (7)$$

423 Radiance and standard deviations values from this study were further divided by c to account for
424 the viewing angle dependency.

425 Figure 5a is a scatterplot of $N_Radiance$ versus N_R_{std} . A strong linear relationship is shown
426 with a correlation of 0.92, suggesting that brighter artificial light sources are typically associated
427 with larger spatial variations in radiance. Figure 5b shows the relationship between N_R_{std} and
428 AOT using a collocated VIIRS DNB and AERONET dataset. Only data from non-winter months
429 (April-October, 2015) were considered. Since nighttime AERONET data are not available, the
430 AERONET data used for the AOT comparisons in Fig. 5b are taken from the day immediately
431 prior and after the VIIRS nighttime observations, following the same collocation method as
432 described in Section 2. Figure 5b shows correlation between N_R_{std} values and collocated
433 AERONET AOTs, and N_R_{std} decreases as AOT increases. As such, Fig. 5b justifies the rationale
434 for retrieving nighttime AOT using spatial variations in artificial light sources.

435

436 **3.2 Parameter quantification for nighttime aerosol optical depth retrievals**

437 As shown in Eq. 6, to retrieve nighttime AOT using VIIRS DNB, ΔI_a , ΔI_{sat} , and k values must
438 be quantified. ΔI_{sat} is the standard deviation of an artificial light source under cloud-free
439 conditions, calculated directly from VIIRS DNB data. ΔI_a is the spatial standard deviation of the

440 same artificial light source but under aerosol and cloud-free conditions. The ΔI_a shall be derived
441 over nights with minimum aerosol contamination, or in principle, from nights with the highest
442 standard deviation of radiance (R_{std}) values. However, given that some of the highest R_{std} values
443 may correspond to unscreened clouds or lightning, for a given year and for a given city we
444 computed the mean ($R_{std_ave}(30\%)$) and standard deviation ($R_{std_std}(30\%)$) of the 30% highest R_{std}
445 values. We then used the mean plus 2 times standard deviation of 30% highest R_{std} values
446 ($R_{std_ave}(30\%) + 2 \times R_{std_std}(30\%)$) to represent the ΔI_a value. Assuming a normal data distribution,
447 two standard deviations above the mean $R_{std_ave}(30\%)$ values should represent the top 1% of the
448 highest R_{std} values of all data points—providing a way to compute the highest R_{std} value while
449 simultaneously minimizing cloud and lightning contamination. Artificial light sources are
450 excluded if the ratio of $R_{std_std}(30\%)$ to $R_{std_ave}(30\%)$ is above 15%. Those artificial light sources
451 with larger variations in peak R_{std} values are likely to be associated with cities that have less stable
452 artificial light signals. Over the US, because of the concerns for ice and snow contamination as
453 mentioned in Sect. 3.1, only data from non-winter months (April-October, 2015) were used. For
454 the India and Middle East regions, snow and ice contamination is likely insignificant and thus data
455 from all months in 2015 were used.

456 As mentioned in Sect. 2.2, k values are computed using a LUT (pre-computed using the 6S
457 radiative transfer model) for dust, smoke, and pollutant aerosols. For simplicity, we assumed the
458 US, Middle East, and India regions were dominated by pollutant, dust, and smoke aerosols,
459 respectively. In future applications, k values (related to aerosol type) shall either be evaluated on
460 a regional basis, following Remer et al. (2005), or derived directly from VIIRS as mentioned in a
461 later section.

462 Cloud contamination is a long-standing challenge to passive-based satellite aerosol research
463 (e.g., Zhang et al., 2005). In this study, the VIIRS cloud product (VCCLO) was used for cloud
464 clearing of the observed VIIRS DNB scenes. However, only VIIRS Infrared channels are applied
465 for cloud detection at night (Godin and Vicente, 2015). Thus, it is possible that low level clouds,
466 unseen by the VIIRS nighttime cloud mask, may still be present in the “cloud-cleared” scenes. To
467 further exclude potential cloud contaminated artificial light sources, we have implemented
468 additional quality control steps. First, it is noted that in the presence of low clouds certain artificial
469 light source patterns may appear differently from clear-sky conditions. Thus, only nights with
470 mean geolocations of the detected artificial light sources that are within 0.02° of multi-night clear
471 sky means are used. This approach, however, will introduce issues for regions with persistent
472 cloud or thick aerosol plume coverage, such as the Uttar Pradesh state of India, which is mentioned
473 later.

474 It was noted in Sect. 3.1 that the radiance and standard deviation of radiance are strongly
475 correlated. As such, for each city and for each year, a regression relationship between radiance
476 and standard deviation of radiance values was constructed by calculating mean and standard
477 deviation of R_{std} for a given radiance range. For a given range of radiance values, R_{std} values that
478 were two standard deviations above the mean R_{std} for that range were discarded as noisy data.
479 After removing these noisy points, the same procedures were repeated to compute the regression
480 between radiance and R_{std} values for each city. The overall mean of R_{std} (R_{std_mean}) for the given
481 artificial light source was also computed. Data were removed if the R_{std} value was above the
482 estimated R_{std} based on radiance values using the above discussed regression plus 0.5 times
483 R_{std_mean} . This step was taken to further remove cloud contaminated data, but may also remove
484 scenes with thick aerosol plumes.

485

486 **3.3 Regional retrievals**

487 One of the goals of this study is to apply the proposed algorithm on a regional scale. A full
488 retrieval and evaluation, using modified schemes as identified from this paper, will be conducted
489 in follow-up research. Here, we present preliminary results conducted on a regional scale for three
490 selected regions in 2015: the US, Middle East, and India. As mentioned previously, only non-
491 winter months were used (April-October) for the US region due to concerns of snow and ice
492 contamination, while all months were included for the other two regions.

493 Figure 6a shows the comparison between retrieved nighttime AOTs from VIIRS DNB and
494 collocated daytime AERONET AOTs ($0.675 \mu\text{m}$) for the selected 200 cities for 2015. Here VIIRS
495 DNB AOTs are retrieved without using the k (diffuse transmittance) correction term mentioned in
496 Sections 2 and 3.2. A total of 368 collocated points are found with a correlation of 0.59. Figure
497 6b shows the collocated CALIOP and VIIRS nighttime AOTs, again using the retrievals without
498 correcting for the diffuse transmittance term. A correlation of 0.47 was found between CALIOP
499 AOT (interpolated to $0.700 \mu\text{m}$) and VIIRS nighttime AOT.

500 Figures 6c and 6d show retrieval comparisons similar to Figs. 6a and 6b, but revised to include
501 the k (diffuse transmittance) correction term. An over correction was found as a higher than 1
502 slope between VIIRS and daytime AERONET AOTs, indicating that the correction for diffuse
503 transmittance may be less important for low aerosol loading cases. The daytime AERONET AOT
504 may not be a fair representation of nighttime AOTs in all cases. Large uncertainties exist in
505 CALIOP extinctions and AOTs as well, due to necessary assumptions of the lidar ratios made in
506 the retrieval process (e.g., Omar et al., 2013). Therefore, significant uncertainties exist in both the
507 AERONET and CALIOP validation sources. Still, this can be improved with the use of nighttime

508 lunar photometry data that is in development from the AERONET group (e.g., Berkoff et al., 2011;
509 Barreto et al., 2013).

510 Figures 7a and 7b show scatter plots of VIIRS DNB AOTs vs. daytime AERONET and
511 nighttime CALIOP AOTs, respectively, for the Middle East for 2015, using retrievals without k .
512 A total of 999 cities were included in the study, and 368 cities were excluded for not passing the
513 stable light source check (or $R_{std_std}(30\%) / R_{std_ave}(30\%) < 15\%$) or not having 3 or more nights
514 that passed the various checks as mentioned in previous sections (both criteria are referred as the
515 stable light source requirement). Note that these criteria may exclude artificial light sources with
516 highly variable day-to-day changes in AOT. A correlation of 0.64 and 0.46 was found between
517 VIIRS and AERONET and CALIOP AOTs, respectively. However, a low bias was clearly present
518 in both comparisons. Figures 7c and 7d show the VIIRS nighttime AOTs versus AERONET (day)
519 and CALIOP (night) AOTs with k included. Similar correlations are found, yet the low bias is
520 largely corrected.

521 A similar study was conducted for India. Here we separated cities in India inside and outside
522 of the Uttar Pradesh (UP) state (retrieval for the UP state is discussed later). Of a total of 2573
523 cities outside of the UP state, 1810 cities were found to satisfy the stable light source requirement.
524 Again, Figs. 8a and 8b are for VIIRS nighttime AOTs versus AERONET adjacent daytime and
525 CALIOP nighttime AOTs without k correction and Figs. 8c and 8d are the plots with the diffuse
526 transmittance (k) correction term included, for cities that were outside the UP state. In all four
527 cases, correlations of around 0.5-0.6 were found, indicating the developed algorithm has
528 reasonable skill in tracking nighttime AOTs. A low bias occurred when k was not included. When
529 k was included, a near 1-to-1 agreement is found in both Figs. 8c and 8d. This exercise reinforces
530 the notion that there is indeed a need to account for diffuse transmittance.

Formatted: Font: Not Italic

531 Figures 9a and 9b compares VIIRS, AERONET, and CALIOP reported AOTs for cities within
532 the UP state of India. Of a total of 421 cities, 326 passed the stable city light requirement.
533 However, a low correlation was found between VIIRS nighttime and daytime AERONET AOTs.
534 This result is not surprising, as thick aerosol plumes cover this region most times of the year, and
535 thus the derived cloud and aerosol free sky standard deviation of the artificial light sources (the
536 ΔI_a values) are not always representative of true aerosol-free cases. Therefore, a longer study
537 period, or careful by-hand analysis, may be needed for deriving ΔI_a values for regions that are
538 known to have persistent thick aerosol plume coverage.

539 Ideally, the retrievals at each light source location should be gridded and averaged to further
540 increase the signal-to-noise ratio. We have tested this concept by averaging retrievals shown in
541 Figs. 6b, 7b, and 8b into a $1^\circ \times 1^\circ$ (Latitude/Longitude) averaged dataset. Artificial light sources
542 that have less than 20 valid nights in a year were excluded to provide statistically robust estimates
543 of ΔI_a . Comparisons of $1^\circ \times 1^\circ$ (Latitude/Longitude) averaged VIIRS DNB AOT retrievals with
544 daytime AERONET data and nighttime CALIOP AOTs are shown in Figs. 6e (6f), 7e (7f), and 8e
545 (8f) for the US, Middle East, and India regions, respectively. Increases in correlations were found
546 between VIIRS and AERONET AOTs for the India regions. Marginal changes in correlations,
547 however, occurred between VIIRS and CALIOP AOTs. Although neither daytime AERONET
548 nor nighttime CALIOP AOTs can be considered as the “ground truth” for nighttime AOTs, these
549 results suggest that the newly developed method has skills in retrieving nighttime AOTs over both
550 dark and bright surfaces.

551 Figure 10 shows nighttime AOT retrievals over India for Jan. 12 and 16 of 2015, with the
552 retrievals from the UP state of India removed. Figures 10a and 10b show true color imagery from
553 Terra MODIS for Jan. 12 and 16, 2015 (obtained from the NASA Worldview through the

554 following site: <https://worldview.earthdata.nasa.gov/>). Figure 10c and 10d show the nighttime
555 images of VIIRS DNB radiance for Jan. 12 and 16, 2015. Over-plotted on Figs. 10a and 10b are
556 retrieved VIIRS nighttime AOTs, with blue, green, orange, and red representing AOT ranges of 0-
557 0.2, 0.2-0.4, 0.4-0.6, and above 0.6, respectively, using gridded data same as used for Figs. 9e-f.
558 Shown in Fig. 10a, on Jan. 12, the west portion of India was relatively aerosol-free, but a heavy
559 aerosol plume is visible around the east coast of India. Similarly, AOTs lower than 0.2 were
560 detected over western India but AOTs larger than 0.6 were found over eastern India. On Jan.16,
561 as indicated from the MODIS daytime image, a thick plume covered the western portion of India,
562 also seen in Fig. 10d via retrieved AOTs above 0.6. Also, the northeast portion of India was
563 relatively aerosol-free as indicated from both MODIS true color imagery (Fig. 10b) and VIIRS
564 nighttime AOT retrievals (Fig. 10d).

565 Based on Figs. 10c and 10d, there were many artificial light sources not used in the retrieval.
566 Those sources were excluded by various quality-control checks of the study due to such reasons
567 as potential cloud contamination, light source instability, or insufficient valid data in a year. It is
568 very likely that some valid data will be removed in this conservative filtering process. New
569 methods must be developed to restore valid data. Some ideas to this effect are presented in the
570 section to follow.

571 The diffuse correction term, k , was shown to be an important factor in reducing bias in these
572 retrievals. We compared the k corrections estimated using the 6S model (Vermote et al., 1997) as
573 well as those empirically derived from this study. By assuming CALIOP nighttime AOTs as the
574 “true” AOTs, and using VIIRS AOTs as shown in Figs. 7b and 8b as inputs, the k correction term
575 could be inferred using Eq. 6. Figure 11a shows the derived k values vs. CALIOP nighttime AOT
576 for the Middle East region. Over-plotted are the k values estimated from the 6S model (Vermote

577 et al., 1997). The two patterns show some agreement, as both the modeled and the empirically
578 derived k values are near or above 1 for CALIOP AOTs of 0.0, and below 0.5 when CALIOP
579 AOTs of ~ 1 . This behavior indicates that the 6S-modeled k correction may provide a reasonable
580 first-order estimate for dust aerosols in this region. Figure 11b shows a similar plot as Fig. 11a
581 but for the India region. A larger data spread was found between the empirically derived and
582 modeled k values assuming smoke aerosols, although the overall patterns were similar. One of the
583 possible reasons for the disparity is that unlike the Middle East region, where dust aerosols
584 dominate, the India region is subject to many other aerosol species including dust and pollutants,
585 occurring across different regions and varying with season.

586

587 **3.5 Limitations and possible improvements**

588 Although showing some skill, the retrieval algorithm examined in this study has its limitations.
589 First, most retrievals are limited to AOTs less than 1.5. This is because scenes with heavy aerosol
590 plumes can either be misclassified as clouds by the VIIRS cloud product, or removed during the
591 additional cloud screening steps introduced in this study. For heavy aerosol plumes, much larger
592 areas could be detected as “light sources” due to enhanced diffuse radiation (e.g., Figure 11), and
593 have different mean geolocations than low aerosol loadings and cloud free nights, and thus would
594 be removed due to the geolocation checks as mentioned in Section 3.2. A data loss, especially for
595 heavy aerosol cases, is experienced in this study due to those stringent data screening steps. Also,
596 for the purpose of avoiding cloud or lightning contamination in this study, ΔI_a values were not
597 derived from nights with the highest radiance or standard deviation of radiance values. Doing so
598 creates a problem for regions having frequent heavy aerosol plume loading, such as the UP state
599 of India.

600 Both issues mentioned above may be mitigated by constructing a prescribed city pattern for
601 each light source based on a multi-night composite from cloud free and low aerosol loading
602 conditions. In that case, light source pixels from the exact same location would be used each night
603 to reduce data loss, especially for nights with heavy aerosol plumes. In constructing the predefined
604 city pattern, ΔI_a values may also be derived. The construction of a prescribed city pattern will be
605 attempted in a future study.

606 Even after vigorous attempts at cloud screening, there remains some cloud contamination.
607 Such conditions may account in Figs. 6-8 for high VIIRS AOT but low CALIOP or AERONET
608 AOT cases, although both daytime AERONET data and CALIOP data have their own issues for
609 representing nighttime aerosol optical depth, as discussed. More advanced cloud screening
610 methods are needed to improve the screening-out of residual clouds. In addition, snow and ice
611 cover pose challenges for this study, and new methods need to be developed to account for snow
612 / ice coverage and allow for attempts at nighttime AOT retrievals over those scenes.

613 Even the algorithm as presented shows skill in retrieving nighttime AOT. Given that there are
614 hundreds of thousands of cities and towns across the world that could serve as sources for this
615 algorithm, the composite of retrievals from artificial light sources may provide a tractable means
616 to attaining regional to global description of nighttime aerosol conditions, on both moonlit and
617 moon-free nights, and over both dark and bright land surfaces. Considering the current glaring
618 nocturnal gap in AOT, the current results show promise for providing closure and thereby enabling
619 cloud/aerosol process studies and improved parameterizations for weather and climate modeling.

620

621 **4 Conclusions and Implications**

622 In this study, based on Visible/Infrared Imager/Radiometer Suite (VIIRS) Day/Night band
623 (DNB) data from 2015, we examined the characteristics of artificial light sources for selected cities
624 in the US, India, and the Middle East regions. Our findings point toward the following key
625 conclusions:

626 1. Radiance from artificial light sources is a function of time of year, lunar illumination and
627 geometry, and viewing geometry. Larger radiance values and spikes in radiance values
628 can occur during the winter season, possibly related to snow and ice cover, indicating the
629 need for careful snow and ice detection for nighttime retrievals using VIIRS data for
630 regions that may experience snow/ice coverage. The normalized radiance increases with
631 lunar fraction, and decreases with increasing lunar zenith angle—as these parameters are
632 tied to the magnitude of downwelling moonlight.

633 2. The normalized standard deviation of artificial light source radiance is a function of time
634 of year and similar to normalized radiance, exhibit spikes during the winter season.
635 However, no significant relationship was found between the normalized standard deviation
636 of radiance and lunar characteristics, including lunar fraction and lunar zenith angle. This
637 finding suggests that the standard deviation of radiance, as opposed to the normalized value
638 of radiance, is a potentially more robust parameter for nighttime aerosol retrievals using
639 VIIRS DNB data.

640 3. Both the normalized radiance and the normalized standard deviation of radiance are a
641 strong function of satellite viewing angle, with larger normalized radiance and the
642 normalized standard deviation of radiance values occurring at higher satellite viewing

Deleted:

644 angles. As anticipated by past research, this viewing angle dependency must be accounted
645 for in VIIRS DNB nighttime aerosol retrievals based on artificial light sources.

646 4. Preliminary evaluations over the US for 200 selected cities, over the Middle East for 999
647 cities/towns, and over India for 2995 cities/towns (excluding the Uttar Pradesh State of
648 India) show reasonable agreements between VIIRS nighttime aerosol optical thickness
649 (AOT) and values estimated by adjacent-daytime Aerosol Robotic Network
650 (AERONET) and nighttime Cloud-Aerosol Lidar with Orthogonal Polarization (CALIOP).
651 This finding suggests that the use of artificial light sources holds the potential of being
652 viable for regional as well as global nighttime aerosol retrievals.

653 5. Poor correlation was found between VIIRS nighttime AOTs and daytime AERONET
654 AOTs for the Uttar Pradesh state in India. This region is frequently covered by thick
655 aerosol plumes, and this may introduce a difficulty in constructing cloud and aerosol free
656 night characteristics of artificial light sources (ΔI_a) for the retrieval process. Based on this
657 finding, we conclude that detailed analysis, and perhaps by-hand selection of non-turbid
658 baseline conditions, is needed for estimating ΔI_a values in regions of climatologically high
659 and persistent turbidity.

660 6. In contrast to McHardy et al. (2015), the need for a diffuse correction in the nighttime
661 aerosol retrieval process was found to indeed be important for regions with heavy aerosol
662 loadings. This study further suggests radiative transfer model based estimations of the
663 diffuse correction term compare reasonably well with empirically derived values over the
664 Middle East where the dominant aerosol type is dust. However, in cases such as the India
665 region, where several aerosol types may be expected during a year, a larger data spread
666 was found, and specification of the diffuse correction term requires additional study.

667 Despite the advances made here, there remain many limitations to the current algorithm. For
668 example, snow, ice, and cloud contamination can significantly affect the retrieved AOTs.
669 Advanced procedures for snow, ice, and cloud removal are needed, with a full evaluation for the
670 potential impacts. Also, high aerosol loading may be screened out due to misclassification of thick
671 aerosol plumes as clouds. A pattern-based artificial light source method will be examined in a
672 future study as one approach to mitigating this issue. Despite these known issues, these low-light
673 studies forge a promising new pathway toward providing nighttime aerosol optical property
674 information on the spatial and temporal time scales of value to the significant needs of the aerosol
675 modeling community in terms of regional to global nighttime aerosol property information.

676 **Acknowledgments:**

677 The support of the Office of Naval Research under grant N00014-16-1-2040 and the NOAA JPSS
678 Program Office are gratefully acknowledged. S. L. Jaker was partially supported by the NASA
679 Grant of NNX17AG52G and NSF project IIA-1355466. The global city base used in this study is
680 a free open source dataset. “This product includes data created by MaxMind, available from
681 <http://www.maxmind.com/>”.

682

683 **References**

- 684 Barreto, A., Cuevas, E., Damiri, B., Guirado, C., Berkoff, T., Berjón, A. J., Hernández, Y.,
685 Almansa, F., and Gil, M.: A new method for nocturnal aerosol measurements with a lunar
686 photometer prototype, *Atmos. Meas. Tech.*, 6, 585-598, doi:10.5194/amt-6-585-2013,
687 2013.
- 688 Berkoff, T. A., Sorokin, M., Stone, T., Eck, T. F., Raymond Hoff, R., Welton, E., Holben, B.:
689 Nocturnal Aerosol Optical Depth Measurements with a Small-Aperture Automated
690 Photometer Using the Moon as a Light Source, *J. Atmos. Ocean. Technol.*, 28, 1297–1306,
691 2011.
- 692 Chen, H., Xiong, X., Sun, C., Chen, X., Chiang, K.: Suomi-NPP VIIRS day–night band on-orbit
693 calibration and performance, *J. Appl. Remote. Sens.*, 11, Article 36019,
694 <https://doi.org/10.1117/1.JRS.11.036019>, 2017.
- 695 [Choo, G. H., & Jeong, M. I. \(2016\). Estimation of nighttime aerosol optical thickness from Suomi-NPP DNB](#)
696 [observations over small cities in Korea. *Korean Journal of Remote Sensing*, 32\(2\), 73-86.](#)
- 697 Elvidge, C. D., Baugh, K., Zhizhin, M., Hsu, F. C., and Ghosh, T.: VIIRS Night-Time Lights,
698 *International Journal of Remote Sensing*, 38, 5860–5879, 2017.
- 699 Godin, R., and Vicente, G.: Joint Polar Satellite System (JPSS) Operational Algorithm Description
700 (OAD) Document for VIIRS Cloud Mask (VCM) Intermediate Product (IP) Software,
701 National Aeronautics and Space Administration (NASA), Greenbelt, Maryland, Goddard
702 Space Flight Center. Access on November 2, 2018
703 ([https://jointmission.gsfc.nasa.gov/sciencedocs/2015-08/474-00062_OAD-VIIRS-Cloud-](https://jointmission.gsfc.nasa.gov/sciencedocs/2015-08/474-00062_OAD-VIIRS-Cloud-Mask-IP_L.pdf)
704 [Mask-IP_L.pdf](#)), 2015.

705 Holben, B. N., Eck, T. F., Slutsker, I., Tanré, D., Buis, J. P., Setzer, A., Vermote, E., Reagan, J.
706 A., Kaufman, Y. J., Nakajima, T., Lavenu, F., Jankowiak, I., and Smirnov, A.: AERONET
707 - A Federated Instrument Network and Data Archive for Aerosol Characterization, *Rem.
708 Sens. Environ.*, 66, 1-16, 1998.

709 Johnson R. S., Zhang J., Reid, J. S., Hyer, E. J., and Miller, S. D.: Toward Nighttime Aerosol
710 Optical Depth Retrievals from the VIIRS Day/Night Band, *Atmos. Meas. Tech.*, 6, 1245-
711 1255, doi:10.5194/amt-6-1245-2013, 2013.

712 Lee, T.E., Miller, S.D., Turk, F.J., Schueler, C., Julian, R., Deyo, S., Dills, P., Wang, S.: The
713 NPOESS VIIRS day/night visible sensor. *Bull. Am. Meteorol. Soc*, 87, 191–199, 2006.

714 McHardy T., Zhang, J., Reid, J. S., Miller, S. D., Hyer, E. J., and Kuehn, R.: An improved method
715 for retrieving nighttime aerosol optical thickness from the VIIRS Day/Night Band, *Atmos.
716 Meas. Tech.*, 8, 4773-4783, doi:10.5194/amt-8-4773-2015, 2015.

717 Miller, S.D., Straka, W., III, Mills, S.P., Elvidge, C.D., Lee, T.F., Solbrig, J., Walther, A.,
718 Heidinger, A.K., Weiss, S.C.: Illuminating the Capabilities of the Suomi National Polar-
719 Orbiting Partnership (NPP) Visible Infrared Imaging Radiometer Suite (VIIRS) Day/Night
720 Band. *Remote Sens.*, 5, 6717–6766, 2013.

721 Mills, S., Weiss, S., and Liang, C.: VIIRS Day/Night Band (DNB) Stray Light Characterization
722 and Correction, *Proceedings SPIE 8866, Earth Observing Systems XVIII*, 88661P,
723 <https://doi.org/10.1117/12.2023107>, 2013.

724 Omar, A. H. and coauthors: CALIOP and AERONET aerosol optical depth comparisons: One size
725 fits none, *Journal of Geophysical Research: Atmospheres*, 118, 4748–4766,
726 doi:10.1002/jgrd.50330, 2013.

727 Remer L. A., Kaufman, Y. J., Tanré, D., Mattoo, S., Chu, D. A., Martins, J. V., Li, R.-R., Ichoku,
728 C., Levy, R. C., Kleidman, R. G., Eck, T. F., Vermote, E., Holben, B. N.: The MODIS
729 Aerosol Algorithm, Products, and Validation, *J. Atmos. Sci.*, 62, pp. 947-973,
730 [10.1175/JAS3385.1](https://doi.org/10.1175/JAS3385.1), 2005.

731 Toth, T. D., Campbell, J. R., Reid, J. S., Tackett, J. L., Vaughan, M. A., Zhang, J., and Marquis,
732 J. W.: Minimum aerosol layer detection sensitivities and their subsequent impacts on
733 aerosol optical thickness retrievals in CALIPSO level 2 data products, *Atmos. Meas. Tech.*,
734 11, 499-514, <https://doi.org/10.5194/amt-11-499-2018>, 2018.

735 Vermote, E. F., Tanré, D., Deuzé, J. L., Herman, M., and Morcrette, J. J.: Second simulation of
736 the satellite signal in the solar spectrum, 6S: an overview, *IEEE Trans. Geosci. Remote
737 Sens.*, 35, 675–686, 1997.

738 [Wang, J., Aegerter, C., Xu, X., & Szykman, J. J. \(2016\). Potential application of VIIRS Day/Night Band for](#)
739 [monitoring nighttime surface PM2.5 air quality from space. Atmospheric Environment, 124, 55-63.](#)

740 Zhang, J., Reid, J. S., and Holben, B. N.: An analysis of potential cloud artifacts in MODIS over
741 ocean aerosol optical thickness products, *Geophysical Research Letters*, VOL. 32, L15803,
742 doi:10.1029/2005GL023254, 2005.

743 Zhang, J., Reid, J. S., Turk, J., and Miller, S.: Strategy for studying nocturnal aerosol optical depth
744 using artificial lights, *International Journal of Remote Sensing*, 29:16, 4599-4613, 2008.

745 Zhang J., Reid, J. S., Campbell, J. R., Hyer, E. J., and Westphal, D. L.: Evaluating the Impact of
746 Multi-Sensor Data Assimilation on A Global Aerosol Particle Transport Model. *J.
747 Geophys. Res. Atmos.*, 119, 4674–4689, doi:[10.1002/2013JD020975](https://doi.org/10.1002/2013JD020975), 2014.

748
749
750

752 **Figure Captions**

753 **Figure 1.** Spatial distribution of (a) 200 cities over the US, b). 999 cities over the Middle East,
754 and c). 2995 cities over India, used in this study. Red dots show cities/towns from the Uttar
755 Pradesh (UP) state of India—a region of climatologically high aerosol loading.

756
757 **Figure 2.** (a) VIIRS DNB contrast-enhanced imagery centered over North America from the
758 VIIRS DNB for October, 1 2015. (b) Same as (a), but with cloud screening and quality assurance
759 steps applied for cloudy (grey), saturated pixels (yellow), and solar zenith angles $< 102^\circ$ (cyan).
760 (c) Similar to (b), but with artificial light sources identified through a granule level detection
761 (orange). (d) Similar to (c) but showing artificial light sources cross checked with a known city
762 database and through a regional level detection (green).

763
764 **Figure 3.** (a) VIIRS nighttime imagery on April 13, 2015 over Sioux City, Iowa, US. b) Similar
765 to (a) but showing detected artificial light sources using data [within \$\pm 0.28^\circ\$ \(Latitude\) and \$\pm 0.295^\circ\$](#)
766 [\(Longitude\) of the city center \(green\), as indicated by the red box](#). Orange colors show the detected
767 artificial light sources through a granule level detection. Only green pixels are utilized for aerosol
768 retrievals.

769
770 **Figure 4.** (a), (c), (e), and (g) show the normalized radiance of artificial light sources (200 selected
771 cities over the US, for 2015) as functions of Julian day, lunar fraction, lunar zenith angle, and
772 satellite zenith angle, respectively. (b), (d), (f), and (h) show the corresponding normalized
773 standard deviation of radiance for artificial light sources. [Cold to warm colors represent data](#)
774 [density from low to high.](#)

Deleted: d
Deleted: within $\pm 0.3^\circ$ (Latitude/Longitude) of the city center (green)

778
779 **Figure 5.** (a) Normalized radiance versus normalized standard deviation of radiance for 200 cities
780 over the US for 2015. (b) The normalized standard deviation of radiance as a function of adjacent
781 daytime AERONET AOT (0.675 μm).

782
783 **Figure 6.** (a) Scatter plot of VIIRS nighttime AOT versus adjacent daytime AERONET AOT
784 (0.675 μm) for 200 selected cities over the US for 2015. No diffuse correction is applied. (b)
785 Similar to (a) but for using nighttime CALIOP AOT (0.7 μm). (c) and (d)) Similar (a) and (b) but
786 with the diffuse correction implemented. (e) and (f): Similar to Figs. 6c and 6d but for gridded
787 VIIRS data (averaged into $1^\circ \times 1^\circ$ Latitude/Longitude grids). Artificial light sources with fewer
788 than 20 nights that passed various cloud screening and QA checks are excluded. [Cold to warm](#)
789 [colors represent data density from low to high.](#)

790
791
792 **Figure 7.** Similar to Fig. 6 but for 999 cities over the Middle East for 2015.

793
794 **Figure 8.** Similar to Fig. 7 but for the India region for 2015. Artificial light sources from the
795 Uttar Pradesh State of India are excluded.

796
797 **Figure 9.** (a) Scatter plot of VIIRS nighttime AOT versus adjacent day time AERONET AOT
798 (0.675 μm) over the Uttar Pradesh State of India for 2015. Diffuse correction is applied. (b):
799 similar to (a), but for using nighttime CALIOP AOT (0.7 μm).

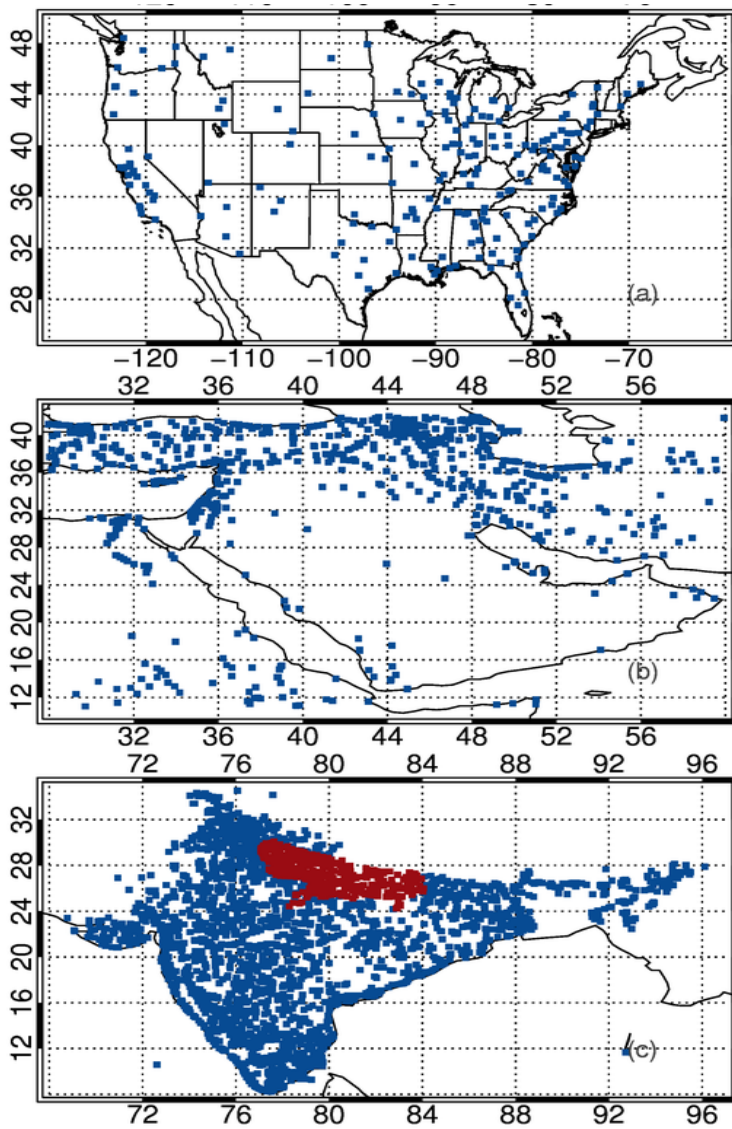
800

801 **Figure 10.** Terra MODIS true color imagery (NASA Worldview) for Jan. 12, 2015 over India.
802 (b): Similar as (a) but for Jan. 16, 2015. (c): VIIRS nighttime imagery on Jan. 12, 2015. Over
803 plotted are VIIRS nighttime AOT retrievals in $1^{\circ}\times 1^{\circ}$ (Latitude/Longitude) grid format. Blue,
804 green, orange, and red colors represent AOT ranges of 0-0.2, 0.2-0.4, 0.4-0.6 and > 0.6 ,
805 respectively. (d) similar to (c) but for Jan. 16, 2015.

806

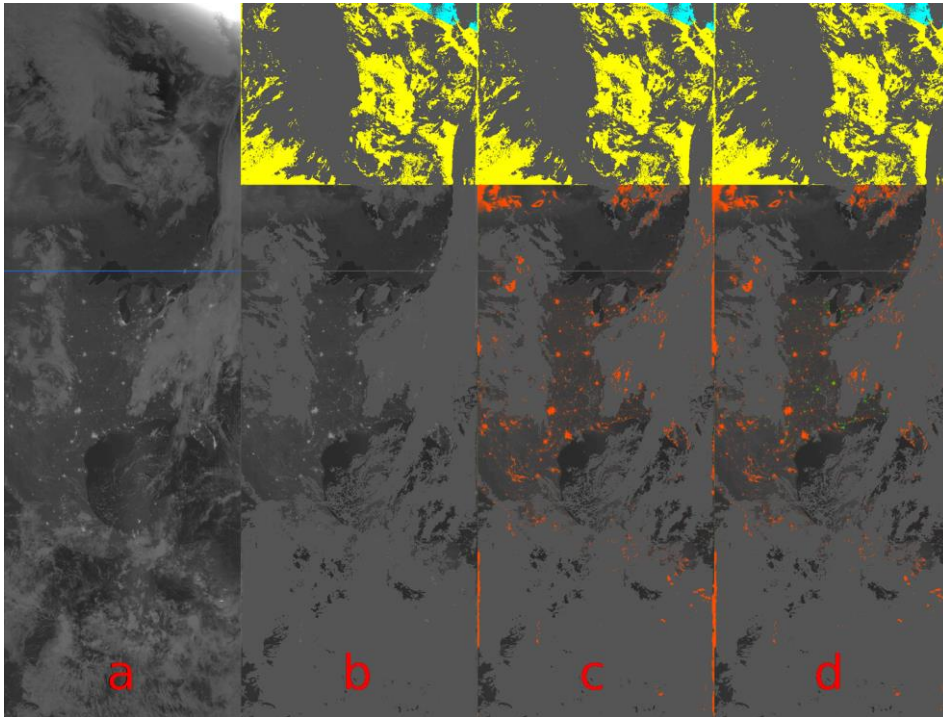
807 **Figure 11.** (a) Empirically derived (using data from Fig. 7d) and 6S model estimated diffuse
808 correction terms for the Middle East for 2015. (b): Similar to Fig. 10a but for the India region for
809 2015 (using data from Fig. 8d).

810



811

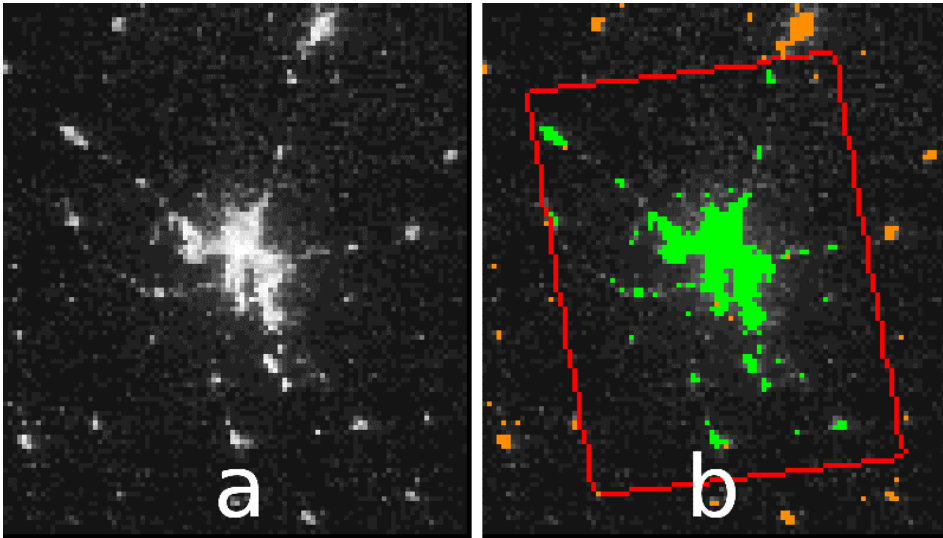
812 **Figure 1.** Spatial distribution of (a) 200 cities over the US, b). 999 cities over the Middle East,
 813 and c) 2995 cities over India, used in this study. Red dots show cities/towns from the Uttar
 814 Pradesh (UP) state of India—a region of climatologically high aerosol loading.



815

816 **Figure 2.** (a) VIIRS DNB contrast-enhanced imagery centered over North America from the
 817 VIIRS DNB for October, 1 2015. (b) Same as (a), but with cloud screening and quality assurance
 818 steps applied for cloudy (grey), saturated pixels (yellow), and solar zenith angle $s < 102^\circ$ (cyan).
 819 (c) Similar to (b), but with artificial light sources identified through a granule level detection
 820 (orange). (d) Similar to (c) but showing artificial light sources cross checked with a known city
 821 database and through a regional level detection (green).

822



823

824

825 **Figure 3.** (a) VIIRS nighttime imagery on April 13, 2015 over Sioux City, Iowa, US. b) Similar
826 to (a) but showing detected artificial light sources using data within $\pm 0.28^\circ$ (Latitude) and $\pm 0.295^\circ$
827 (Longitude) of the city center (green), as indicated by the red box. Orange colors show the detected
828 artificial light sources through a granule level detection. Only green pixels are utilized for aerosol
829 retrievals.

830

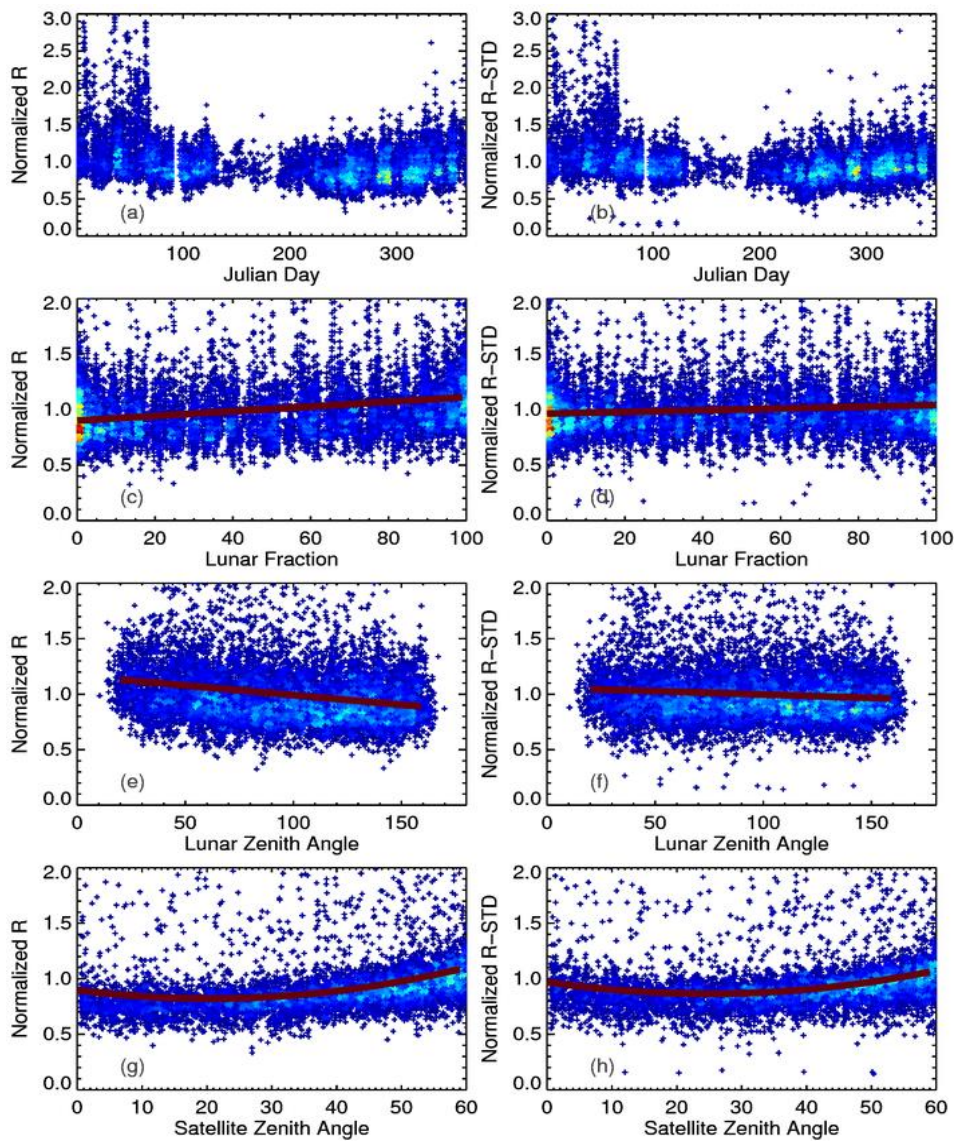
831

832

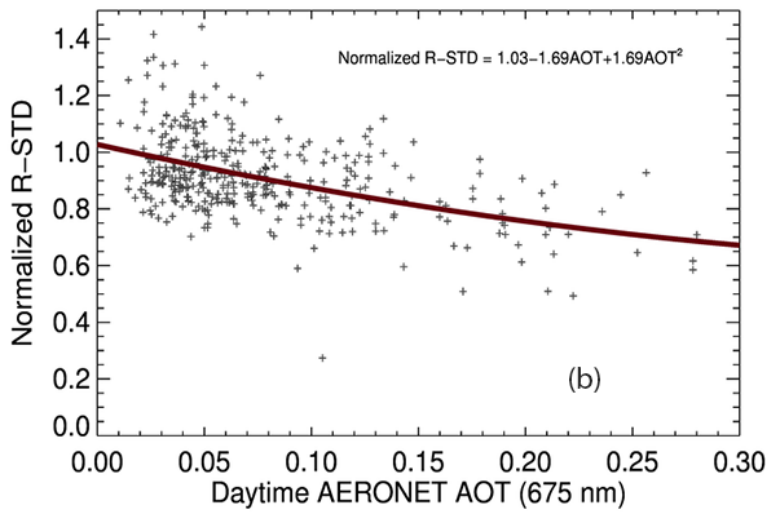
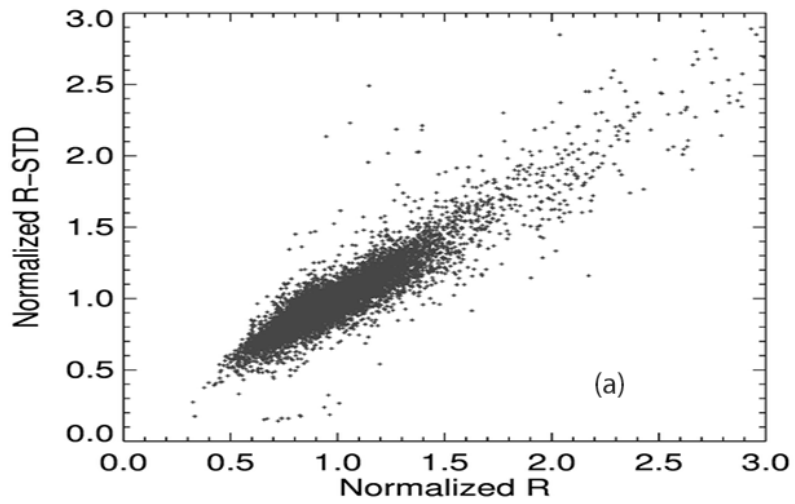
833

834

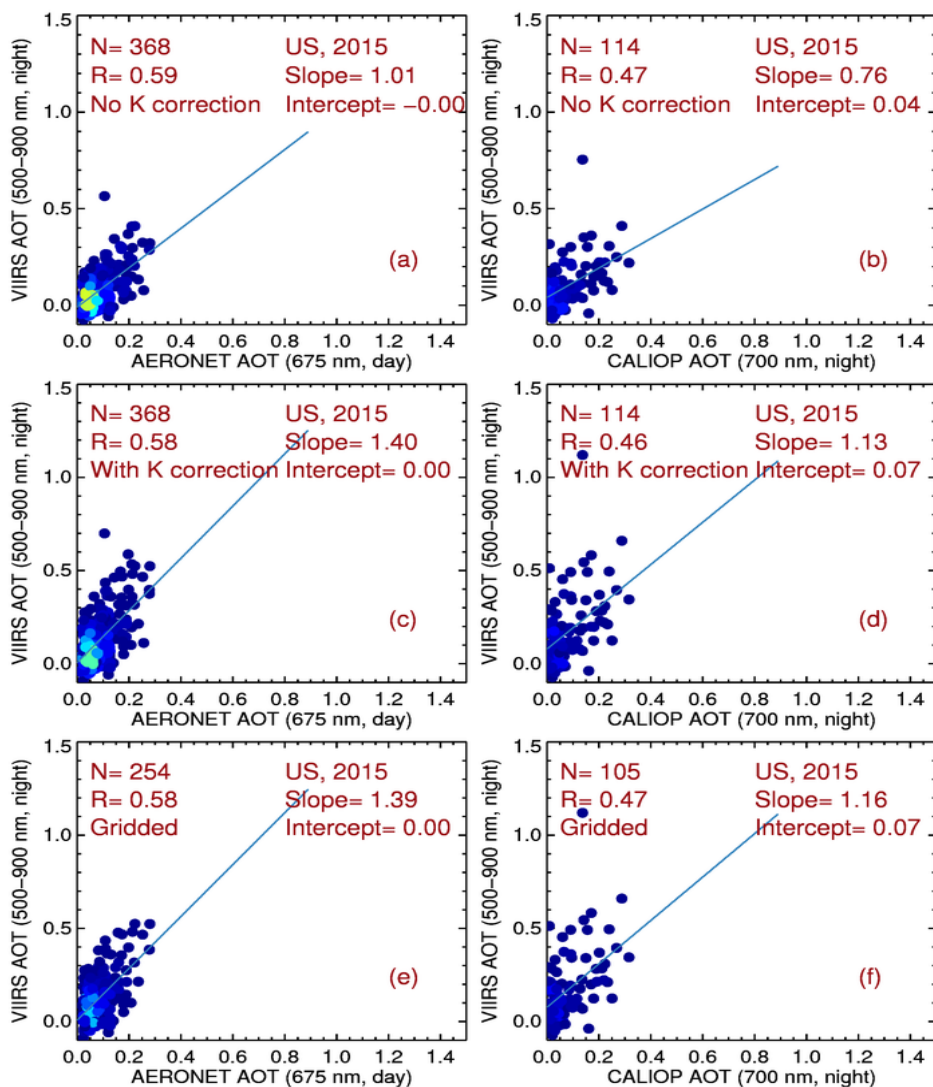
Deleted: d



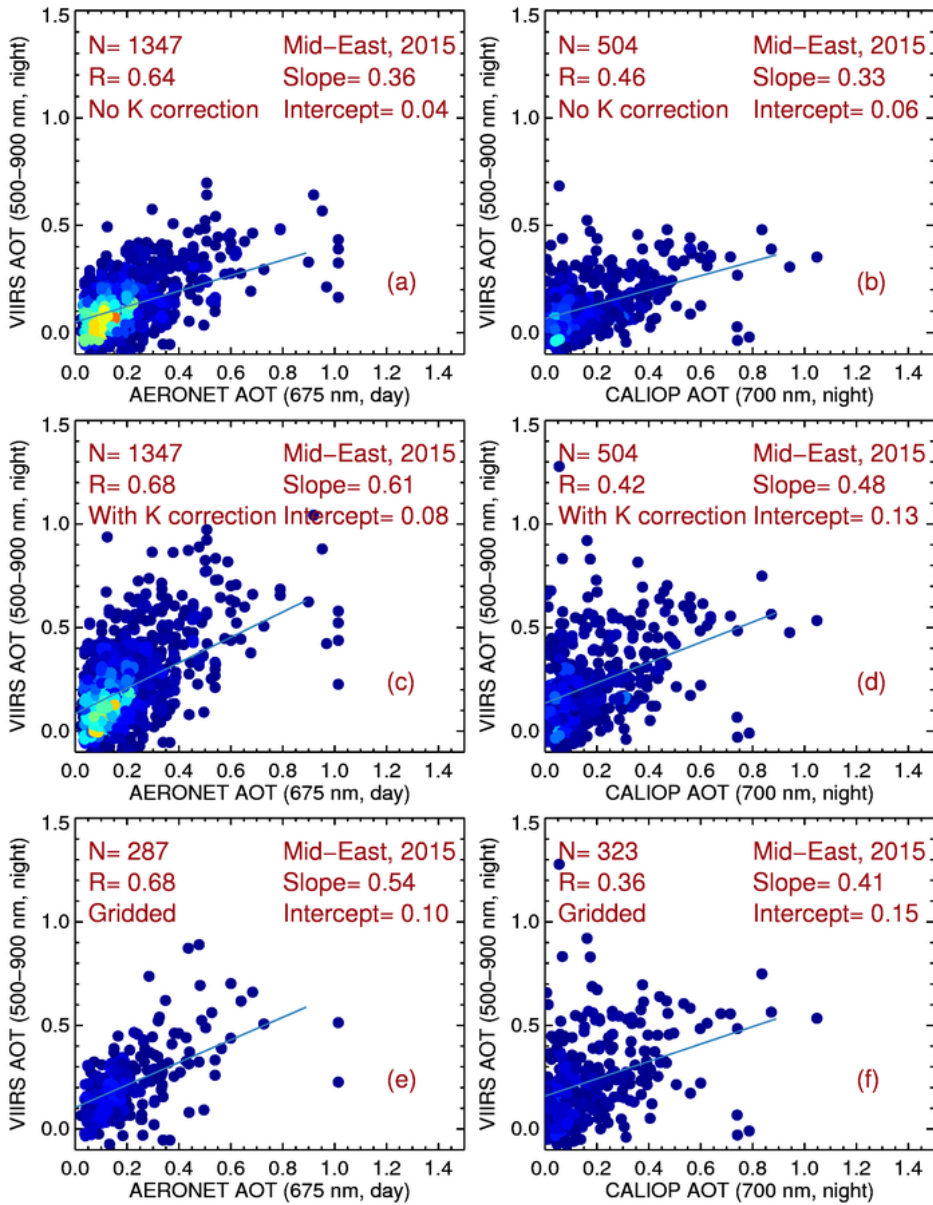
836
 837 **Figure 4.** (a), (c), (e), and (g) show the normalized radiance of artificial light sources (200 selected
 838 cities over the US, for 2015) as functions of Julian day, lunar fraction, lunar zenith angle, and
 839 satellite zenith angle, respectively. (b), (d), (f), and (h) show the corresponding normalized
 840 standard deviation of radiance for artificial light sources. [Cold to warm colors represent data](#)
 841 [density from low to high.](#)

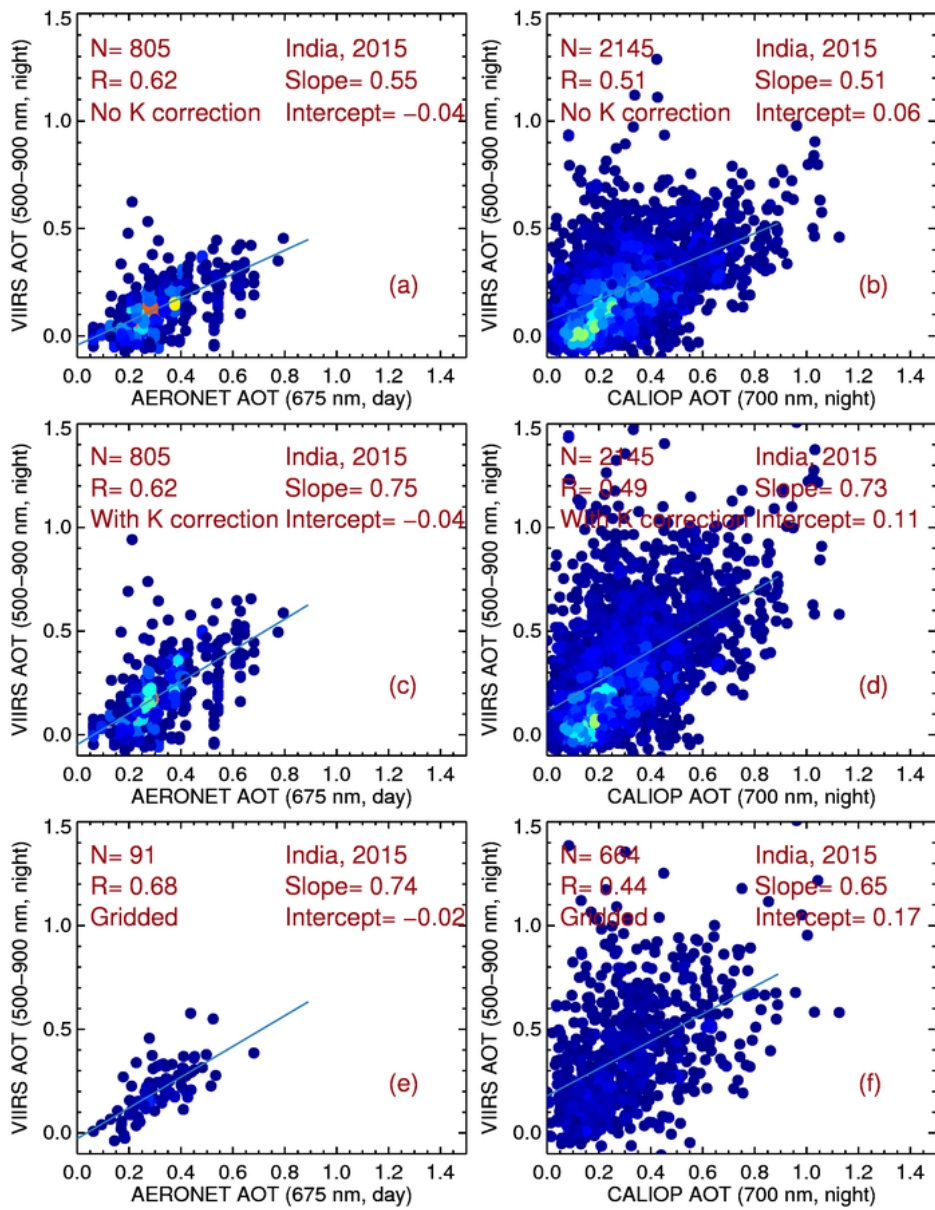


842
 843 **Figure 5.** (a) Normalized radiance versus normalized standard deviation of radiance for 200 cities
 844 over the US for 2015. (b) The normalized standard deviation of radiance as a function of adjacent
 845 daytime AERONET AOT (0.675 μm).

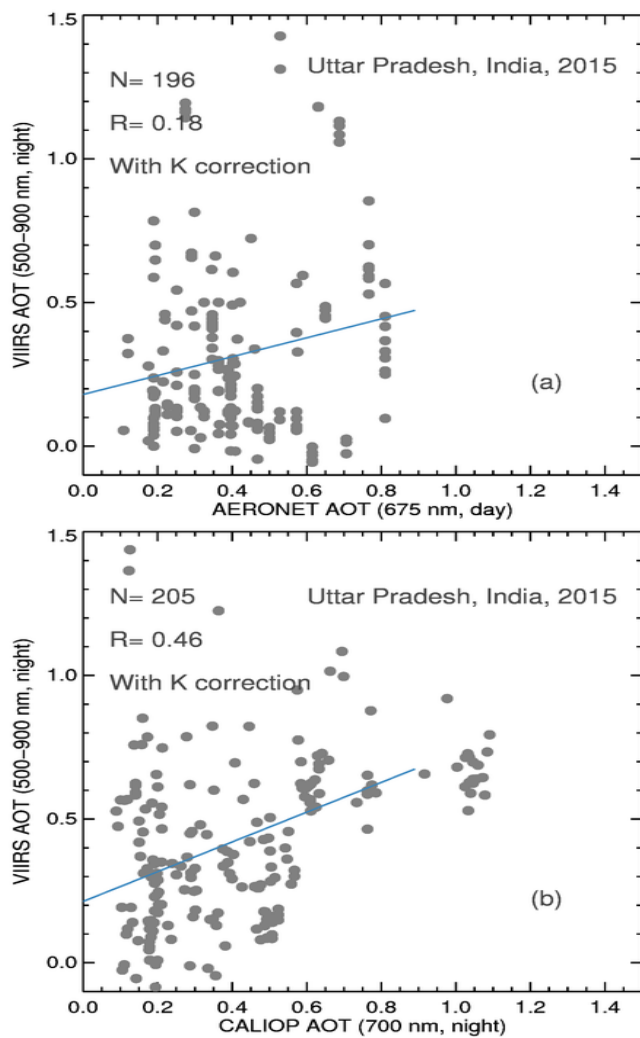


846
 847 **Figure 6.** (a) Scatter plot of VIIRS nighttime AOT versus adjacent daytime AERONET AOT
 848 (0.675 μm) for 200 selected cities over the US for 2015. No diffuse correction is applied. b)
 849 Similar to (a) but for using nighttime CALIOP AOT (0.7 μm). (c) and (d) Similar (a) and (b) but
 850 with the diffuse correction implemented. (e) and (f): Similar to Figs. 6c and 6d but for gridded
 851 VIIRS data (averaged into $1^\circ \times 1^\circ$ Latitude/Longitude grids). Artificial light sources with fewer
 852 than 20 nights that passed various cloud screening and QA checks are excluded. [Cold to warm](#)
 853 [colors represent data density from low to high.](#)

856 **Figure 7.** Similar to Fig. 6 but for 999 cities over the Middle East for 2015.



857
 858 **Figure 8.** Similar to Fig. 7 but for the India region for 2015. Artificial light sources from the
 859 Uttar Pradesh State of India are excluded.
 860



862

863

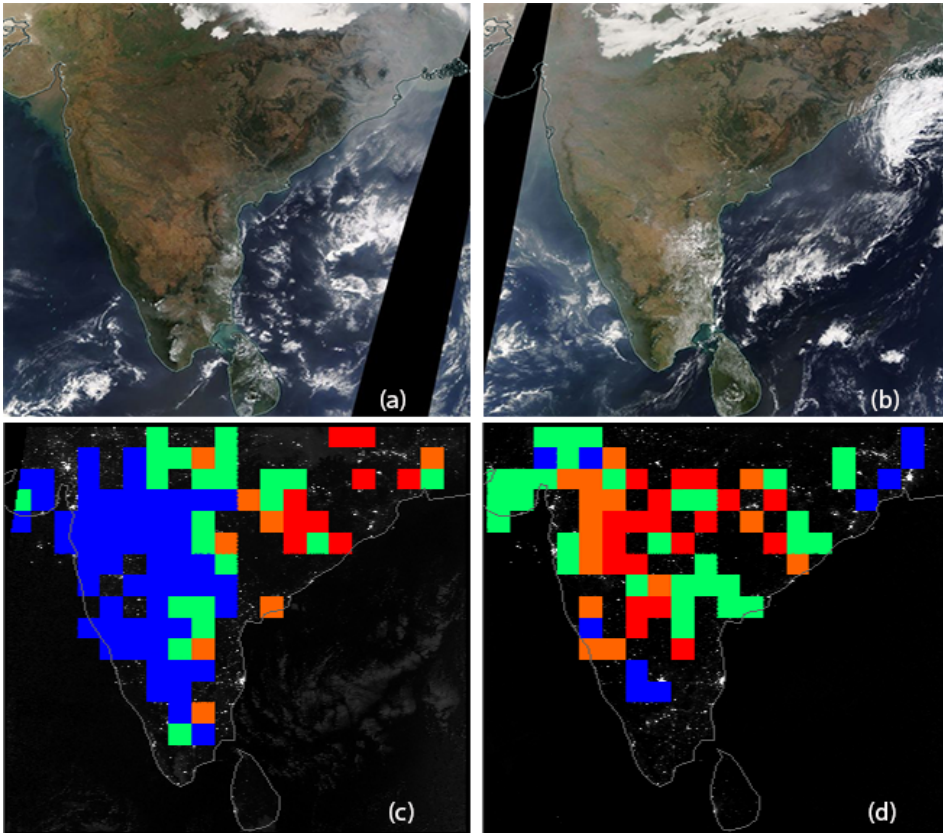
864

865

866

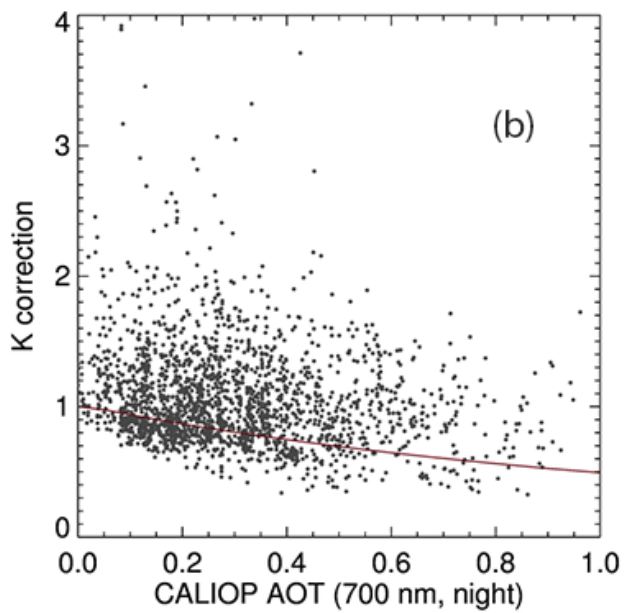
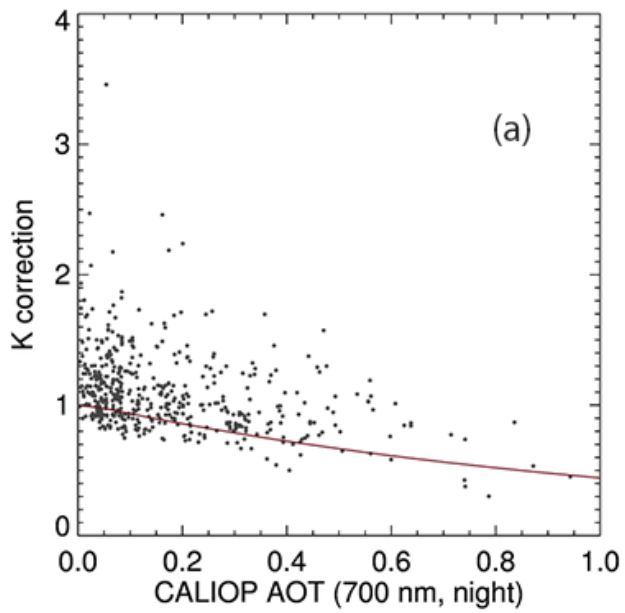
867

Figure 9. (a) Scatter plot of VIIRS nighttime AOT versus adjacent day time AERONET AOT (0.675 μm) over the Uttar Pradesh State of India for 2015. Diffuse correction is applied. (b): similar to (a), but for using nighttime CALIOP AOT (0.7 μm).



868
 869 **Figure 10.** Terra MODIS true color imagery (NASA Worldview) for Jan. 12, 2015 over India.
 870 (b): Similar as (a) but for Jan. 16, 2015. (c): VIIRS nighttime imagery on Jan. 12, 2015. Over
 871 plotted are VIIRS nighttime AOT retrievals in $1^{\circ} \times 1^{\circ}$ (Latitude/Longitude) grid format. Blue,
 872 green, orange, and red colors represent AOT ranges of 0-0.2, 0.2-0.4, 0.4-0.6 and > 0.6 ,
 873 respectively. (d) similar to (c) but for Jan. 16, 2015.
 874

875



877 **Figure 11.** (a) Empirically derived (using data from Fig. 7d) and 6S model estimated diffuse
878 correction terms for the Middle East for 2015. (b): Similar to Fig. 10a but for the India region for
879 2015 (using data from Fig. 8d).